UNIVERSITY of WORCESTER Worcester Research and Publications

Title A calmodulin-binding transcription factor links calcium signaling to antiviral RNAi defense in plants

Item Type	Journal Article (Version of Record)
UoW Affiliated Authors	Hong, Yiguo
Full Citation	Wang, Y., Gong, Q., Wu, Y., Huang, F., Ismayil, A., Zhang, D., Li, H., Gu, H., Ludman, M., Fátyol, K., Qi, Y., Yoshioka, K., Hanley-Bowdoin, L., Hong, Yiguo and Liu, Y. (2021) A calmodulin-binding transcription factor links calcium signaling to antiviral RNAi defense in plants. Cell Host & Microbe. ISSN 1931-3128
DOI/ISBN/ISSN	https://doi.org/10.1016/j.chom.2021.07.003
Journal/Publisher	Cell Press Elsevier
Rights/Publisher Set Statement	© 2021 Elsevier Inc. Open archive. Made available under an Elsevier user license Articles published under an Elsevier user license are protected by copyright. Users may access, download, copy, translate, text and data mine (but may not redistribute, display or adapt) the articles for non-commercial purposes. Full Licence: https://www.elsevier.com/en-gb/about/policies-and-standards/open-access-licenses/elsevier-user
License	This is a non commercial license where the use of published articles for commercial purposes is prohibited.
Link	https://www.sciencedirect.com/science/article/pii/S1931312821003048#!

For more information, please contact library-research@worc.ac.uk

Article

Cell Host & Microbe

A calmodulin-binding transcription factor links calcium signaling to antiviral RNAi defense in plants

Graphical abstract

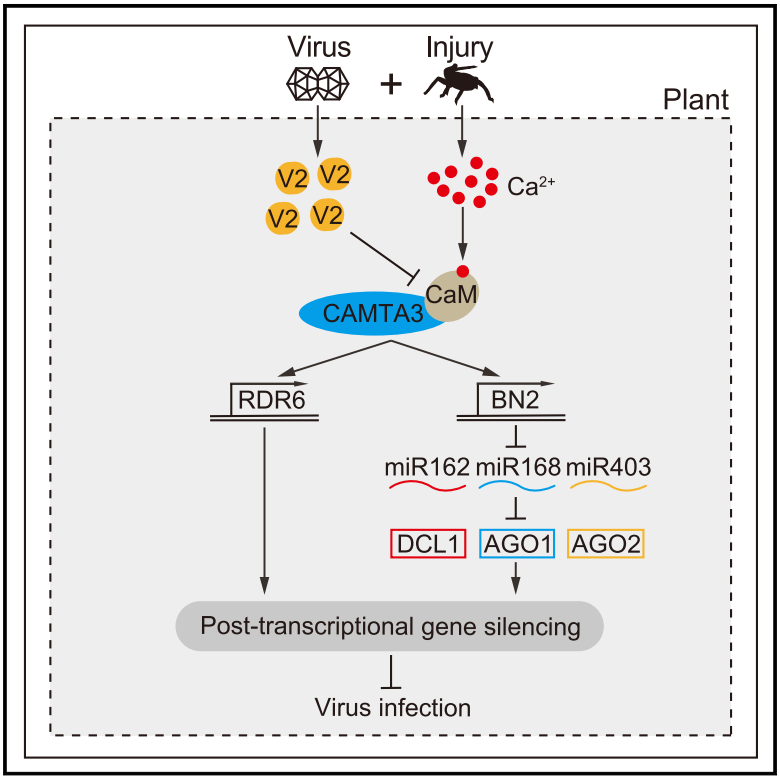

Authors

Yunjing Wang, Qian Gong, Yuyao Wu, ..., Linda Hanley-Bowdoin, Yiguo Hong, Yule Liu

Correspondence

yuleliu@mail.tsinghua.edu.cn

In brief

Little is known about the initial signal to trigger RNAi gene expression and how RNAi is transcriptionally regulated during virus infection. Wang et al. reveal that wounding triggers Ca^{2+} → CaMs → CAMTA3 → BN2/RDR6 signaling cascade to induce RNAi gene expression, priming antiviral RNAi defense. Geminivirus V2 proteins suppress this pathway to promote viral infection.

Highlights

- Plants recognize wounding-triggered Ca^{2+} flux to prime antiviral RNAi defense
- CAMTA3 activates *RDR6*/*BN2* expression to enhance antiviral RNAi
- BN2 upregulates *AGO1/2* and *DCL1* RNA levels by degrading miRNAs
- Geminivirus proteins disrupt CaM-CAMTA3 interaction to suppress antiviral RNAi

Wang et al., 2021, Cell Host & Microbe *29*, 1393–1406
September 8, 2021 © 2021 Elsevier Inc.
https://doi.org/10.1016/j.chom.2021.07.003

CellPress

Cell Host & Microbe

CellPress

Article

A calmodulin-binding transcription factor links calcium signaling to antiviral RNAi defense in plants

Yunjing Wang,[1,2,9] Qian Gong,[1,2,9] Yuyao Wu,[1,2] Fan Huang,[1,2] Asigul Ismayil,[1,2] Danfeng Zhang,[1,2] Huangai Li,[1,2] Hanqing Gu,[1,2] Márta Ludman,[3] Károly Fátyol,[3] Yijun Qi,[1,2] Keiko Yoshioka,[4] Linda Hanley-Bowdoin,[5] Yiguo Hong,[6,7,8] and Yule Liu[1,2,10,*]

[1]MOE Key Laboratory of Bioinformatics and Center for Plant Biology, School of Life Sciences, Tsinghua University, Beijing 100084, China
[2]Tsinghua-Peking Center for Life Sciences, Beijing 100084, China
[3]Institute of Genetics and Biotechnology, Hungarian University of Agriculture and Life Sciences, Szent-Györgyi Albert u. 4, Gödöllő 2100, Hungary
[4]Department of Cell and Systems Biology, University of Toronto, 25 Willcocks Street, Toronto, ON M5S 3B2, Canada
[5]Department of Plant and Microbial Biology, North Carolina State University, Raleigh NC 27695, USA
[6]Research Centre for Plant RNA Signaling, College of Life and Environmental Sciences, Hangzhou Normal University, Hangzhou 311121, China
[7]School of Life Sciences, University of Warwick, Coventry CV4 7AL, UK
[8]School of Science and the Environment, University of Worcester, Worcester WR2 6AJ, UK
[9]These authors contributed equally
[10]Lead contact
*Correspondence: yuleliu@mail.tsinghua.edu.cn
https://doi.org/10.1016/j.chom.2021.07.003

SUMMARY

RNA interference (RNAi) is an across-kingdom gene regulatory and defense mechanism. However, little is known about how organisms sense initial cues to mobilize RNAi. Here, we show that wounding to *Nicotiana benthamiana* cells during virus intrusion activates RNAi-related gene expression through calcium signaling. A rapid wound-induced elevation in calcium fluxes triggers calmodulin-dependent activation of calmodulin-binding transcription activator-3 (CAMTA3), which activates *RNA-dependent RNA polymerase-6* and *Bifunctional nuclease-2* (*BN2*) transcription. BN2 stabilizes mRNAs encoding key components of RNAi machinery, notably *AGONAUTE1/2* and *DICER-LIKE1*, by degrading their cognate microRNAs. Consequently, multiple RNAi genes are primed for combating virus invasion. *Calmodulin-*, *CAMTA3-*, or *BN2*-knockdown/knockout plants show increased susceptibility to geminivirus, cucumovirus, and potyvirus. Notably, Geminivirus V2 protein can disrupt the calmodulin-CAMTA3 interaction to counteract RNAi defense. These findings link Ca^{2+} signaling to RNAi and reveal versatility of host antiviral defense and viral counter-defense.

INTRODUCTION

Viral pathogens cause yield and nutritious losses in crops. To counterattack, plants have evolved multilayered mechanisms including physical barriers, *R*-gene-mediated defense, and RNA interference (RNAi) (Soosaar et al., 2005). RNAi is an across-kingdom innate immunity and gene regulatory machinery; its molecular framework has been well characterized. Plants employ dicer-like endoribonucleases (DCLs) to cleave structural or double-stranded (ds) RNA derived from single-stranded (ss) molecules by RNA-dependent RNA polymerase 6 (RDR6) into small interfering RNAs (siRNAs). One strand of the siRNA duplex is then loaded into an RNA-induced silencing complex (RISC), which contains RNase H-like Argonautes (e.g., AGO1/2), and guides AGO to cleave homologous target RNAs, such as viral RNAs (Fang and Qi, 2016; Wilson and Doudna, 2013). Interestingly, viral infection often activates and upregulates expression of multiple RNAi-related genes in plants (Bai et al., 2012; Qin et al., 2018; Vargas-Salinas et al., 2021), but its initial cue is largely unknown. Moreover, it also remains unclear how RNAi genes are transcriptionally regulated, although posttranscriptional control for some RNAi genes has been described (Allen et al., 2005; Yang et al., 2020).

To overcome cellular physical barriers such as cuticle and cell wall, plant viruses invade cells through touching of plants or transmission by vectors including insects, nematodes, and fungi (Nicaise, 2014). Plant cells respond to this abiotic wounding with changes in cytosolic calcium (Ca^{2+}) concentration and activation of Ca^{2+}-signaling pathways (Toyota et al., 2018; Yan et al., 2018). Such specific Ca^{2+} change, so called "Ca^{2+} signature," is decoded and relayed by Ca^{2+} sensors such as calmodulin (CaM). CaMs consist of 4 EF-hand motifs that chelate Ca^{2+}, which causes conformational changes leading to interaction between activated CaMs and their target proteins (Babu et al., 1988). CaM exerts a regulatory role in plant immunity by interacting with target proteins including CaM-binding transcription activator-3 (CAMTA3) (DeFalco et al., 2016; Galon et al., 2010). CAMTA3 regulates homeostasis of the plant-defense-associated

hormone salicylic acid (SA) and plays a crucial role in stress responses (Du et al., 2009; Wang et al., 2009). Moreover, CAMTA3 binds to the rapid stress response element (RSRE) in the promoters of stress-regulated genes and is a positive regulator of early stress responses (Benn et al., 2016, 2014; Bjornson et al., 2014; Walley et al., 2007). However, no link has been made between the Ca^{2+}-CaM-CAMTA3 signaling cascade and RNAi antiviral defense. Further, it is unknown whether and how the wounding can act as the initial cue to prime antiviral RNAi to combat viral infection during or/and just after a virus first enters a plant cell.

RESULTS

CaM is a positive RNAi regulator

During our yeast two-hybrid screening of partners that may interact with viral silencing suppressor (VSR) V2, we identified CaM3, a Ca^{2+}-binding protein in *Nicotiana benthamiana* (see below). There is a very high amino acid sequence identity among CaMs (Figure S1A). To investigate whether *CaMs* participate in RNAi, we performed *CaMs*-knockdown (KD) using *Tobacco rattle virus* (TRV)-induced gene silencing (VIGS) with a *CaM3* gene fragment (Figures S1B and S1C). *CaMs*-KD plants displayed abnormal phenotypes including dwarfism and severe leaf curling (Figure S1B) because multiple *CaMs* were silenced in *CaMs*-KD plants as indicated by qRT-PCR assay (Figure S1C). 16c lines are transgenic *N. benthamiana* plants constitutively and highly expressing green fluorescent protein (GFP) and have widely been used to visualize the actions of small RNAs and measure RNA silencing level (Ruiz et al., 1998). We then tested whether *CaM3*-KD affected RNAi in 16c plants by co-delivering *GFP* dsRNA construct to induce systemic *GFP* silencing. Expression of *GFP* transgene was suppressed in upper young leaves of control versus *CaM3*-KD plants (Figure S1D). *GFP* mRNA and protein levels were approximately 2.58- or 1.75-fold higher in *CaM3*-KD plants, respectively, while *GFP* siRNAs accumulated about 6.25 times higher in control plants (Figures S1E–S1G). These data suggest that *CaM3*-KD impairs RNAi in plants.

To affirm the role of CaMs in RNAi, we co-expressed myelocytomatosis (MYC)-tagged CaM3 (MYC-CaM3) or C-terminal luciferase (MYC-cLUC) with GFP in *N. benthamiana* and 16c plants. At 3 days post-agroinoculation, GFP fluorescence was weaker in leaves overexpressing MYC-CaM3 versus MYC-cLUC (Figure S1H), consistent with the levels of *GFP* mRNA, siRNA and protein as well as *CaM3* mRNA, which increased in leaves overexpressing MYC-CaM3 compared with MYC-cLUC (Figures S1I–S1L). Overexpression of MYC-CaM1 or MYC-CaM6 had a similar impact on *GFP* silencing (Figures S1M and S1N). Hence, CaM3 and its homologs positively regulate RNAi.

CAMTA3-mediated upregulation of RNAi requires CaM

To understand how CaM3 functions in RNAi, we identified CAMTA3 as a CaM3-interacting partner through affinity purification using MYC-Trap followed by mass spectrometry analysis (Figure S1O). CAMTA3 was further verified to interact with CaM3 via the CaM-binding domain of CAMTA3 (CaMBD) *in vivo* and *in vitro* (Figures S1P–S1R). The *in vitro* pull-down assay also indicated that CAMTA3-CaM3 interaction was Ca^{2+} dependent and severely attenuated by ethylene glycol tetraacetic acid (EGTA), a Ca^{2+} chelator (Figure S1R), raising a question on whether *CAMTA3* is required for RNAi. To address this, we generated *CAMTA3*-knockout (KO) *camta3* plants via CRISPR-Cas9 gene editing (Figures S2A–S2C). *CAMTA3*-KO resulted in increased GFP fluorescence, mRNA, and protein levels but caused a decreased biogenesis of *GFP* siRNAs in plants after transient *GFP* expression (Figures 1A–1D). Further, *CAMTA3*-KO impaired systemic *GFP* RNAi in upper leaves of 16c plants after transient *GFP* expression in the infiltrated leaves (Figures 1E–1H). Meanwhile, *GFP* mRNA and protein levels were lower, but siRNA level was higher when hemagglutinin (HA)-tagged CAMTA3 (HA-CAMTA3) was overexpressed in leaves compared with controls (Figures 1I–1L). Moreover, the K979E mutation in CAMTA3 compromised its interaction with CaM3 (Figures S1S–S1U) and its activity in mediating RNAi (Figure 1I–1L), suggesting that CaM3-CAMTA3 interaction was required to regulate RNAi.

CAMTA3 binds to and activates the *RDR6* promoter

Considering that CAMTA3 is a transcription factor, we performed RNA-seq-based genome-wide transcriptional analysis to identify potential CAMTA3-regulated genes (Figure S2E). We found that *RDR6, AGO1/2*, and *DCL1* were downregulated in *camta3* (Figure S2E). qRT-PCR results confirmed that *RDR6, AGO1/2*, and *DCL1* were downregulated in *camta3* and *CaM3*-KD plants, but upregulated in plants transiently overexpressing *CAMTA3* or *CaM3* (Figures 2A, 2B, and S2F–S2I). We hypothesized that CAMTA3 controls expression of these genes to modulate RNAi. Through analyzing the promoter sequence of downregulated genes, we identified a CGCG motif in the *RDR6* promoter, which might be a binding site for CAMTA3 (Nie et al., 2012). This prediction was confirmed by yeast one-hybrid assay, ChIP-qPCR and electrophoretic mobility shift assay (EMSA) (Figures 2C–2E). We co-expressed CAMTA3 with a luciferase (LUC) reporter under the control of the *RDR6* promoter ($RDR6_{pro}$) or its CGCG box mutant ($RDR6M_{pro}$) (Figures 2G–2I). CAMTA3 enhanced transcription from $RDR6_{pro}$ but not $RDR6M_{pro}$. Similar results were obtained from LUC assays in *N. benthamiana* protoplasts (Figures 2K and 2L). These data demonstrate that CAMTA3 binds to *RDR6* promoter and activates *RDR6* transcription.

CAMTA3-mediated activation of *BN2* transcription intensifies RNAi

No CGCG box/motif was found in the promoter of *AGO1/2* or *DCL1*, implying CAMTA3 does not directly regulate their transcription. We combined our RNA-seq data with VIGS screen and identified *Bifunctional nuclease-2* (*BN2*), a potential small RNA (sRNA) degradation enzyme as hinted (Ramachandran and Chen, 2008), linked it to *CAMTA3*-mediated regulation of *AGO1/2* or *DCL1* expression. *BN2* was downregulated in *camta3*, but upregulated in plants transiently overexpressing HA-CAMTA3 (Figures 2A, 2B, and S2E). The *BN2* promoter contains a CGCG box and CAMTA3 stimulated transcriptional activity of the *BN2* promoter (*BN2pro*) but not a CGCG-box-mutated promoter (*BN2Mpro*) (Figures 2C, 2D, 2F–2H, 2J, 2K,

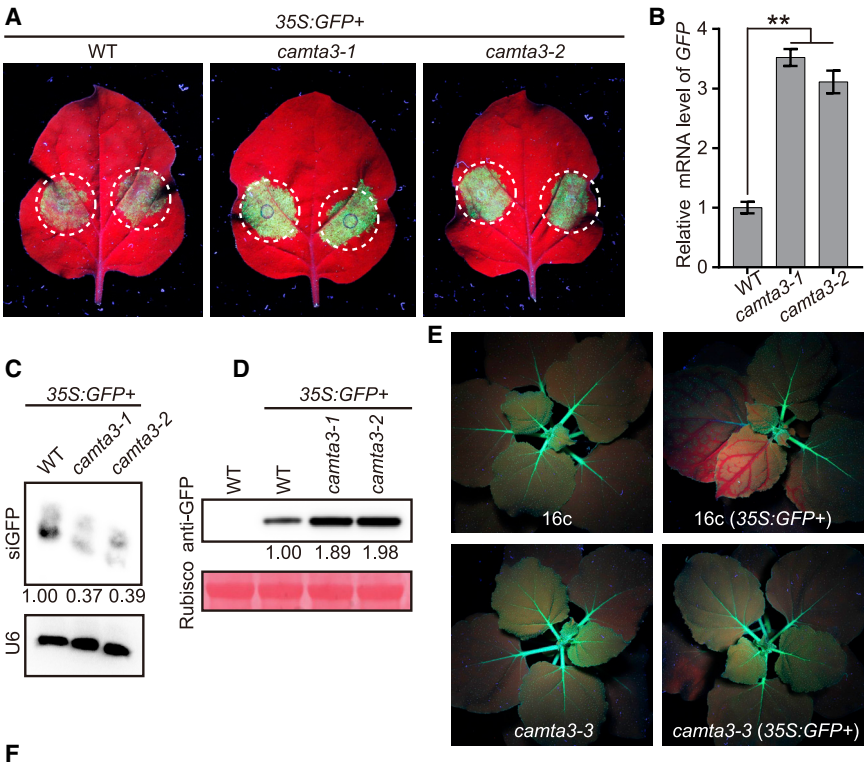

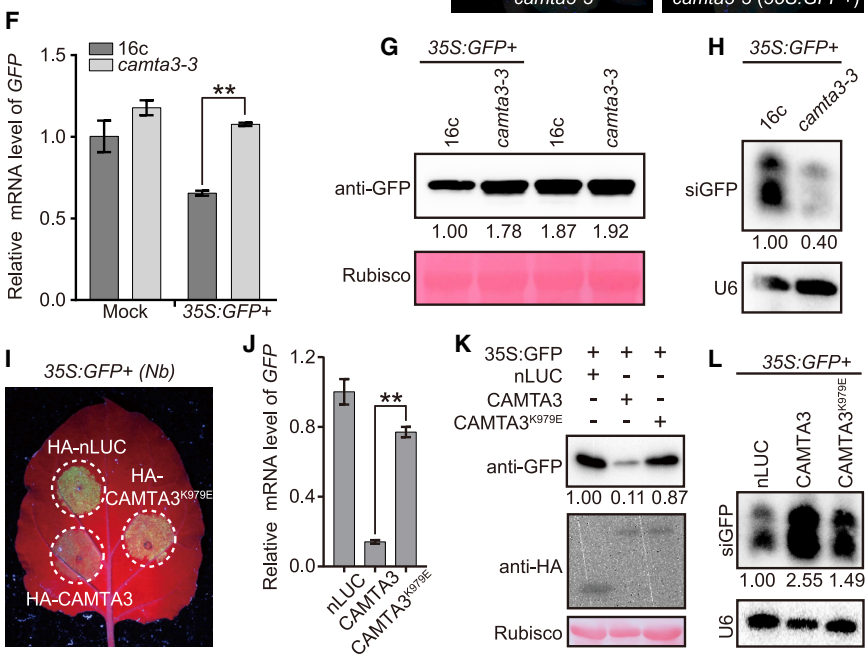

Figure 1. CAMTA3 positively regulates RNAi

(A–D) Transient expression of *GFP* in *camta3-1*, *camta3-2*, or *N. benthamiana* (A). qRT-PCR analysis of relative *GFP* mRNA levels (B), small RNA blot of *GFP*-derived siRNAs (C), and immunoblot assay of GFP proteins (D).

(E–H) *Camta3-3* or 16c *N. benthamiana* plants were inoculated with 35S: GFP and the upper systemic leaves were observed for GFP expression. Photographs were taken under UV light at 20 days post infiltration (dpi) (E). qRT-PCR assays of the relative *GFP* mRNA levels (F). GFP protein levels (G) and *GFP*-derived siRNAs (H).

(I–L) Transient co-expression of HA-nLUC, HA-CAMTA3 or HA-CAMTA3^{K979E} with GFP in *N. benthamiana*. Photographs were taken under UV light at 3 days post infiltration (I). qRT-PCR assay of relative *GFP* mRNA levels (J), immunoblot assay of GFP protein levels (K), and small RNA blot of *GFP*-derived siRNAs (L) in HA-nLUC, HA-CAMTA3 or HA-CAMTA3^{K979E} inoculated plants. Data are mean ± SD, asterisks in qRT-PCR data panels indicate a significant difference (Student's t test, *$p < 0.05$; **$p < 0.01$). The ratios in protein or siRNA levels were analyzed by ImageJ and shown under relevant blots. See also Figure S1.

and 2M). CRISPR-Cas9-mediated *BN2*-KO plants (*bn2*) showed more intense GFP fluorescence and higher *GFP* mRNA and protein levels, but fewer *GFP*-derived siRNAs than controls after transient *GFP* expression (Figures S2D and S2L–S2O). *BN2* overexpression enhanced *GFP* RNAi (Figures S2P–S2S) and upregulated the mRNA levels of *AGO1/2* and *DCL1* but not *RDR6* (Figure S2J). *AGO1/2* and *DCL1* transcript levels but not those of *RDR6* were reduced in *bn2* plants (Figure S2K). We suggest that CAMTA3 indirectly influences mRNA levels of *AGO1/2* or *DCL1* via its transcriptional activation of *BN2*.

BN2 degrades *AGO1/2*- and *DCL1*-targeting miRNAs

We speculate that BN2 might affect mRNA levels of *AGO1*, *AGO2*, and *DCL1* by a sRNAs-mediated mechanism based on the following information. First, *DCL1*, *AGO1*, and *AGO2* mRNAs are targeted by miR162, miR168, and miR403 in plants including *N. benthamiana* (Allen et al., 2005; Pertermann et al., 2018; Vaucheret et al., 2004; Wu et al., 2015; Xie et al., 2003). Second, BN2 is a potential nuclease. Third, ribonucleases are reported to degrade sRNAs *in vitro* and limit their accumulation *in vivo* (Ramachandran and Chen, 2008). To test whether BN2 indeed degrades sRNAs including microRNAs, we performed sRNA-seq to examine how *BN2* affects microRNA accumulation (Table S1). We found that levels of miR162, miR168, and miR403 increased in *bn2* sRNA-seq. We confirmed this result by qRT-PCR and sRNA Northern blots in *bn2* and *camta3* plants (Figures 3A, 3B, and 3E). On the other hand, lysate and glutathione S-transferase (GST) alone showed no nuclease activity (Figures 3C and 3D, lanes 1–2). However, GST-tagged BN2 (GST-BN2) degraded mature miRNAs miR162, miR168, and miR403 (Figures 3C and 3D, lanes 4–6). The GST-BN2M with Ala-substitutions at Glu-143 and Asp-144 in the putative nuclease motif partially lost the nuclease

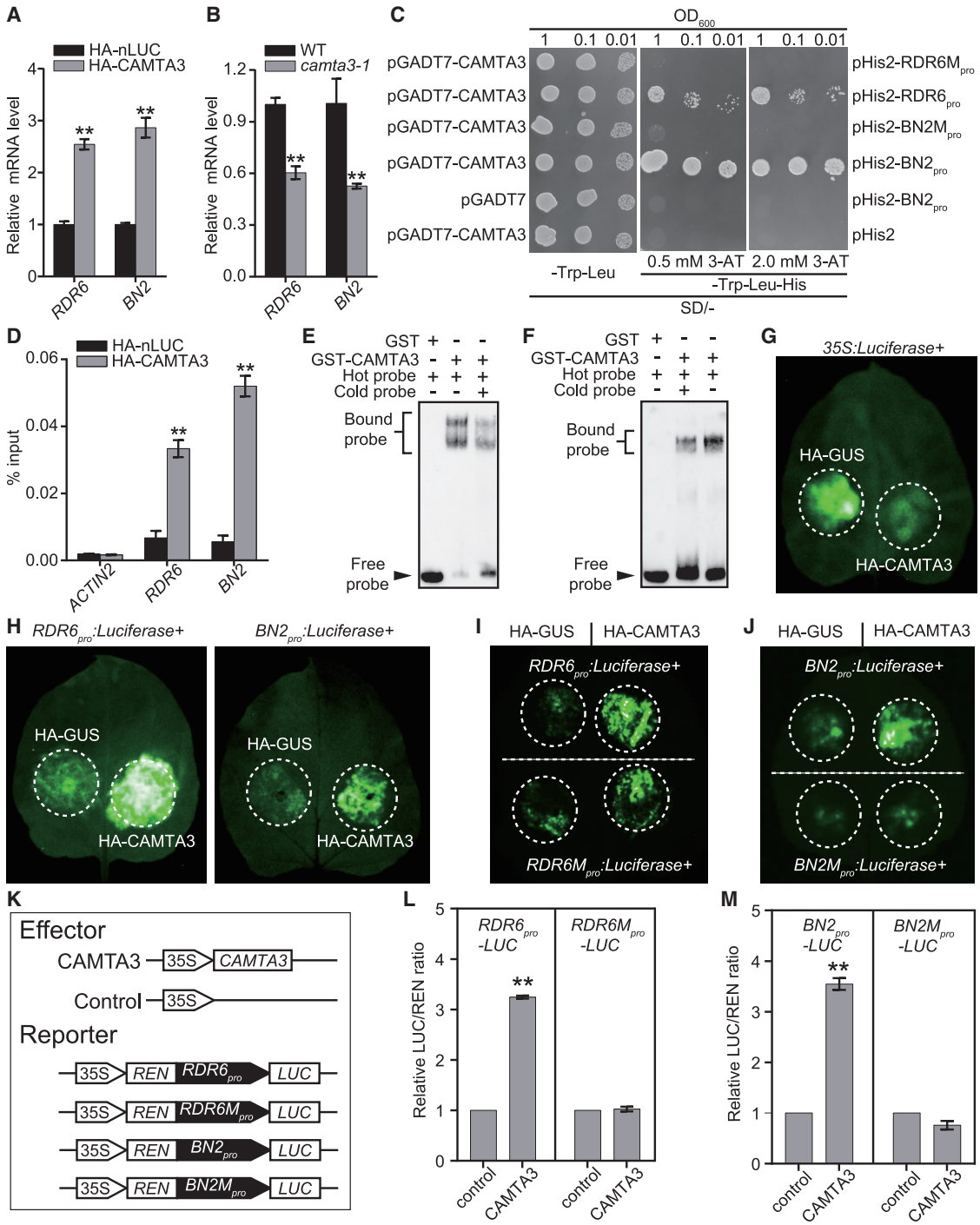

Figure 2. CAMTA3 binds to and activates *RDR6*/*BN2* promoter

(A and B) qRT-PCR assays of *RDR6* and *BN2* mRNA levels in HA-nLUC, HA-CAMTA3 transient overexpression or in wild-type and *camta3-1* leaves.

(C) Yeast one-hybrid assay. Yeast cells were co-transformed with an effector vector containing the $RDR6_{pro}$, $RDR6M_{pro}$ or $BN2_{pro}$, $BN2M_{pro}$ fused to a *pHis2* vector and a prey vector encoding *CAMTA3* fused to pGADT7.

(D) *In planta* ChIP-qPCR. Chromatin from plants expressing HA-CAMTA3 or HA-nLUC were immunoprecipitated and amplified with promoter-specific primers.

(E and F) *In vitro* EMSA. Hot or cold probe is the biotinlabeled or unlabeled CGCG box DNA of $RDR6_{pro}$ (E), $BN2_{pro}$ (F), respectively.

(G–J) CAMTA3-mediated activation of transcription. Expression of luciferase reporter was under the control of the 35S promoter (G), wild-type (H), or mutant (I and J) *RDR6* and *BN2* promoters respectively. The photographs were taken 30 h post infiltration (hpi).

(K) Schematic diagram of the transient luciferase reporter constructs in *N. benthamiana* protoplasts. (L and M) Transient luciferase measurement in *N. benthamiana* protoplasts. Data are mean ± SD, asterisks in data panels indicate a significant difference (Student's t test, *p < 0.05; **p < 0.01). See also Figure S2.

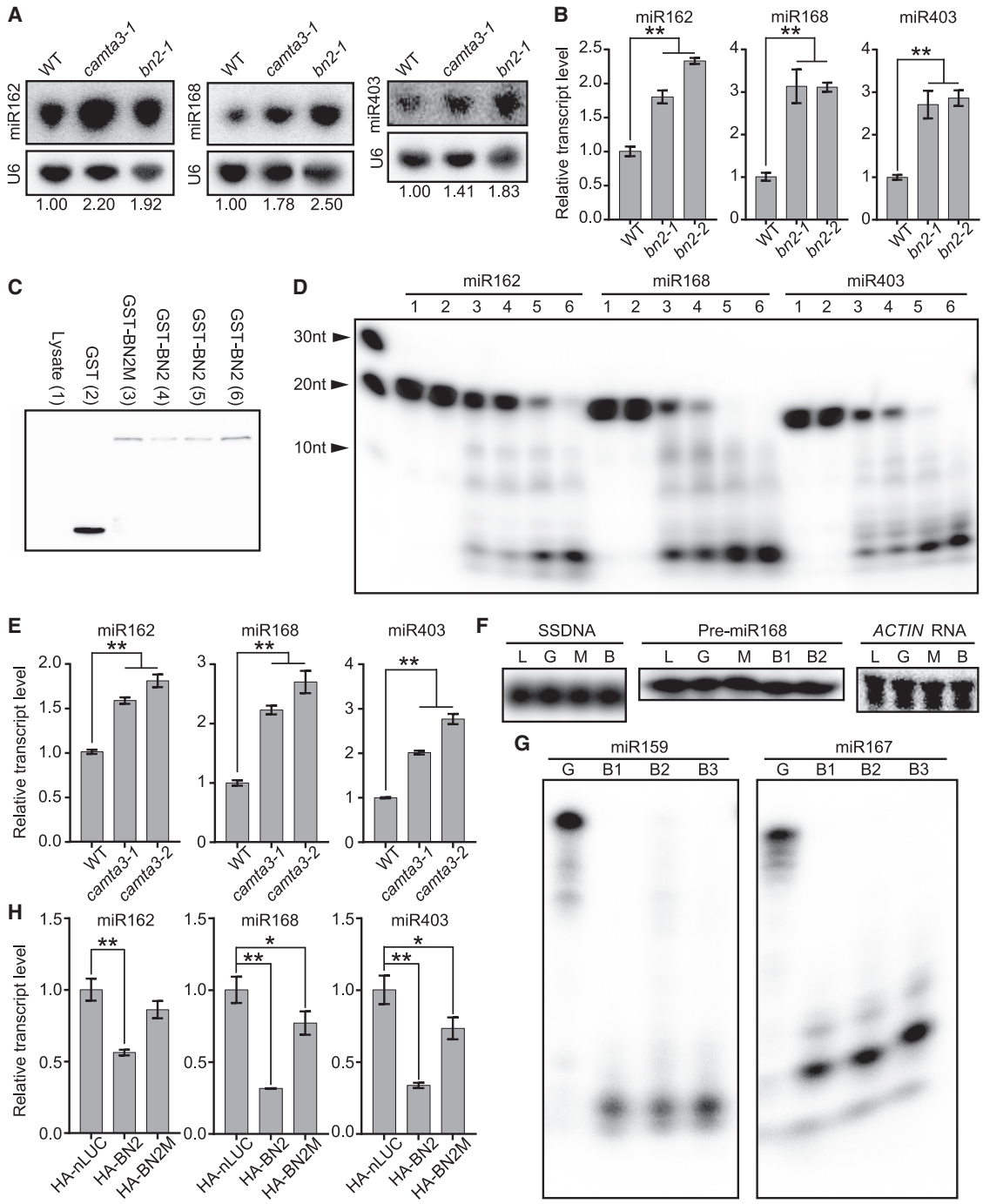

Figure 3. BN2 degrades AGO1/2- and DCL1-targeting miRNAs

(A) Small RNA blot assay of miR162, miR168, and miR403 levels in *camta3-1*, *bn2-1*, and wild-type (WT) *N. benthamiana* plants.

(B) qRT-PCR detection of the relative miR162, miR168, and miR403 levels in *bn2* and wild-type *N. benthamiana*.

(C) Immunoblot assay of recombinant proteins GST, different amount of GST-BN2, or GST-BN2M. The amount of GST and GST-BN2M were 160 and 60 ng, respectively. The amount of GST-BN2 were 20 (lane 4), 40 (lane 5), and 60 ng (lane 6).

(D) Enzymatic activity assays on single-stranded (ss) microRNAs *in vitro*. RNA oligonucleotides were incubated with buffer alone (lane 1), purified GST (lane 2), GST-BN2M (lane 3), or different amount of GST-BN2 (lanes 4–6) as shown in (C).

(E) qRT-PCR detection of the relative miR162, miR168, and miR403 levels in *camta3* and wild-type *N. benthamiana*.

(F) ssDNA oligonucleotide, *in vitro* transcribed 5′ end-labeled pre-miR168 and *in vitro* transcribed 5′ end-labeled *ACTIN* RNA were, respectively, incubated with lysate buffer (L), GST (G), GST-BN2M (M), GST-BN2 (B, B1, or B2). The amount of GST and GST-BN2M were 160 and 60 ng, respectively. The amounts of GST-BN2 were 20 (lane B or B1) and 40 ng (lane B2).

(legend continued on next page)

activity (Figures 3C and 3D, lane 3). GST-BN2 had no effect on ssDNA, pre-miR168 or longer (600 nt) *ACTIN* RNA (Figure 3F) but was able to cleave miR159 and miR167 (Figure 3G), suggesting that BN2 specifically targets and degrades mature miRNAs in a miRNA non-specific manner *in vitro*. We transiently co-expressed *BN2* or *BN2M* with *pre-miRNA162*, *pre-miRNA168*, and *pre-miRNA403* in plants. *BN2* overexpression decreased the amount of mature miR162, miR168, and miR403 by 44%–68%, but *BN2M* overexpression reduced these microRNAs by only 14%–27% (Figure 3H). Thus, BN2 acts as a ribonuclease to degrade microRNAs post-transcriptionally and indirectly regulates the level of *DCL1* or *AGO1/2* mRNA in plants.

CaM3, *CAMTA3*, and *BN2* are required for plant antiviral defense

To test the relevance of the Ca^{2+}→CaMs→CAMTA3→BN2/RDR6→RNAi signaling cascade to virus-plant interactions, we inoculated *camta3*, *bn2*, *RDR6*-KD, and wild-type *N. benthamiana* plants with *Cotton leaf curl Multan geminivirus* (CLCuMuV). CLCuMuV caused more severe symptoms in *camta3* and *bn2* than wild-type plants (Figures 4A and 4C). More viral genomic DNA and vsiRNAs accumulated in the *camta3* and *bn2* plants, as indicated by gel blot, respectively (Figures 4B and 4D). *CAMTA3*-KO or *RDR6*-KD increased the accumulation of CLCuMuV genomic DNA and CLCuMuV-derived vsiRNAs (Figures S3A–S3C), compromised CLCuMuV-mediated RNAi of an endogenous gene *phytoene desaturase* (*PDS*) and *PDS*-derived siRNA accumulation (Figures S3A and S3D), suggesting that *CAMTA3* and *RDR6* are required for both geminivirus-induced gene silencing and plant antiviral defense. We also tested the effect of *CaMs* on CLCuMuV infection by using *Cotton leaf curl Multan betasatellite* (CLCuMuB)-based VIGS plus CLCuMuV as a helper virus (Jia et al., 2016). *CaMs*-KD plants showed more severe viral symptoms and more viral DNA accumulation than control plants (Figures S3F–S3H). In contrast, transgenic plants overexpressing *MYC-CaM3* showed milder viral symptom with reduced viral DNA accumulation than *MYC-GUS* plants (Figures S3I–S3L).

We further tested the role of *CAMTA3* and *BN2* in RNA virus infection by inoculating *camta3*, *bn2*, and wild-type *N. benthamiana* plants with *cucumber mosaic virus* (CMV) (Wang et al., 2011b) with $2b_{N81}$ deficiency (retained N-terminal 81 amino acids of 2b, CMV-$\Delta 2b_{N81}$) and *Plum pox potyvirus* (PPV-GFP) (Ying et al., 2010). Similar to DNA viruses, both CMV-$\Delta 2b_{N81}$ and PPV-GFP showed more severe symptoms, increased levels of viral RNA, and changed quantity of vsiRNA in *camta3* and *bn2* plants (Figures S4A–S4D and S5A–S5D).

To examine if CAMTA3 enhances antiviral defense by activating one or more unknown genes unnecessary for RNAi-dependent antiviral defense, we compared viral symptom, the accumulation of both DNA and RNA viruses, and their cognate vsiRNAs between the *rdr6*/*camta3* double mutants and single mutants. The *RDR6*-KO (*rdr6*) plants were generated as described (Ludman and Fátyol, 2019). For this purpose, we knocked down *CAMTA3* in wild-type and *rdr6* mutant plants by TRV-based VIGS (Liu et al., 2002b). It is worth noting that *RDR6*-KO has no effect on TRV-mediated gene silencing as indicated by using *PDS* reporter gene (Figure S3E) (Liu et al., 2002a; Vaistij and Jones, 2009). Like *camta3* mutant, *CAMTA3*-KD showed more severe viral symptom along with more virus accumulation of both DNA and RNA viruses, suggesting that *CAMTA3*-KD mimics *camta3* mutant plants (Figures 4, S3, S4, and S5). The *camta3*/*rdr6* double mutant plants and *rdr6* single mutant plants showed no difference in viral symptom, accumulation of both DNA and RNA viruses and their cognate vsiRNAs (Figures 4E–4I, S4E–S4I, and S5E–S5I). These altered vsiRNA profiles in *rdr6* background were consistent with previous reports (Aregger et al., 2012; Vaistij and Jones, 2009; Wang et al., 2011b). These experiments indicate that CAMTA3 acts dependently on antiviral RNAi against virus.

Our results demonstrate that plant antiviral defense involves a signal transduction pathway that begins with Ca^{2+}, is sensed by CaMs and the transcriptional activator CAMTA3, and affects transcription of *BN2* and *RDR6* to intensify RNAi.

Geminiviral V2 interferes with CaM3-CAMTA3 interaction to suppress RNAi

CaM3 was identified as a CLCuMuV V2-interacting protein (Figures S6A–S6D). We showed that (1) MYC-CaM3 co-immunoprecipitated with GFP-V2 but not GFP (Figure S6A), (2) bimolecular yellow fluorescence complementation was visible only in V2-nYFP/cYFP-NbCaM3 co-infiltration (Figure S6B), and (3) *in vitro* pull-down assay showed a direct interaction between CaM3 and V2 (Figure S6C). Luciferase complementation imaging assay indicated that V2 also interacted with other CaMs (Figure S6D).

We found that the Arg52 residue in the viral V2 protein is key for interaction with CaM3. The alanine substitution mutation, $V2^{R52A}$, reduced V2 interaction with CaM3 (Figures S6E–S6H) and weakened the V2 ability to suppress RNA silencing (Figure S6I–S6L), suggesting that the interaction between V2 and CaMs is required for V2-mediated RNAi suppression. Further, GFP expression levels are similar between *camta3-1* plants co-expressing $V2^{R52A}$ and V2 (Figures S6M–S6P). Additionally, no difference in GFP expression level is observed between V2-expressing *camta3-1* and V2-expressing wild-type *N. benthamiana* leaves (Figures S6M–S6P). These results suggest that V2 functions to suppress RNAi by disrupting CAMTA3-CaMs interaction. Furthermore, the CLCuMuV-$V2^{R52A}$ mutant virus caused less severe symptom and less viral DNA accumulation than wild-type CLCuMuV (Figures S6Q–S6S). Moreover, *camta3-1* plants supported higher accumulation of CLCuMuV-$V2^{R52A}$ and partially complemented the effect of R52A mutation in V2 on viral accumulation (Figure S6S), suggesting that V2 also functions to suppress antiviral RNAi regulated by CaMs and CAMTA3 in the context of the viral infection.

To gain insight into how the interaction between V2 and CaM impacts suppression of RNAi, we expressed and purified MBP-tagged V2, $V2^{R52A}$, GFP proteins, His-CaM3, and GST-CAMTA3

(G) Degradation of miR159 and miR167 by BN2 *in vitro*. RNA oligonucleotides were incubated with purified GST (G) or GST-BN2 (B1∼3). The amount of GST was 160 ng, and the amounts of GST-BN2 were 20 (lane B1), 40 (lane B2), and 60 ng (lane B3).

(H) qRT-PCR detection of the relative miR162, miR168, and miR403 levels in HA-BN2 or HA-BN2M transient expression leaves. Data are mean ± SD, asterisks in qRT-PCR data panels indicate a significant difference (Student's t test, *$p < 0.05$; **$p < 0.01$). The ratios in siRNA levels were normalized against U6 by ImageJ and shown under relevant blots. See also Table S1.

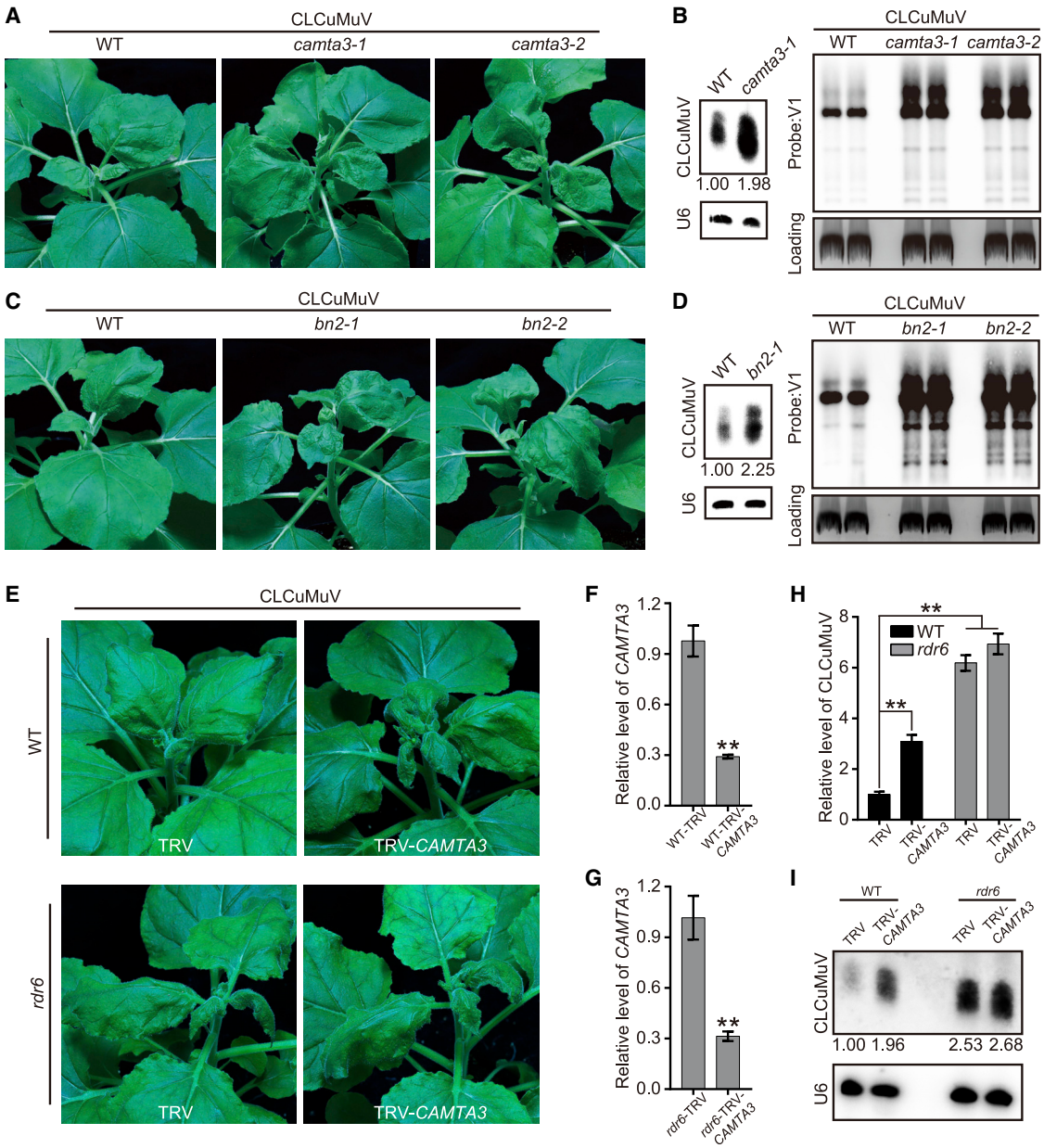

Figure 4. *CAMTA3* and *BN2* are required for antiviral RNAi defense against CLCuMuV

(A and C) Viral symptoms in *camta3, bn2*, and *N. benthamiana* plants infected with CLCuMuV at 16 dpi.

(B and D) Viral-derived siRNAs and viral DNA accumulation in *camta3-1, bn2-1*, and *N. benthamiana* plants. A partial CLCuMuV *V2* DNA was used as a template to make siRNAs probes, partial CLCuMuV *V1* DNA was used as a template to make southern blot probes.

(E–I) Analysis of antiviral RNAi against CLCuMuV in *camta3/rdr6* double and *rdr6* single mutants. The effect of *CAMTA3*-KD on viral symptoms in WT or *rdr6* plants infected with CLCuMuV (E), the level of *CAMTA3* mRNA in wild-type (F) and *rdr6* (G) plants, and the accumulation of CLCuMuV DNA (H) or siRNAs (I) in CLCuMuV-infected systemic leaves of WT or *rdr6* plants. *CAMTA3*-KD was induced by TRV-*CAMTA3* to mimic *camta3* mutant while the empty vector TRV was used as negative control in these experiments. Plants were photographed at 16 days post inoculation. Data are mean ± SD, asterisks in qRT-PCR and qPCR data panels indicate a significant difference (Student's t test, *$p < 0.05$; **$p < 0.01$). The ratios in siRNA levels were analyzed by ImageJ and shown under relevant blots. See also Figures S3–S5.

CaMBD from *E. coli*. We found that less GST-CaMBD was pulled down by histidine-tagged CaM3 (His-CaM3) in the presence of myelin basic protein (MBP)-tagged V2 (MBP-V2) in a dose-dependent manner, but not MBP-GFP and MBP-V2^{R52A} (Figure S7A). Bimolecular fluorescence complementation (BiFC) assays showed that HA-tagged V2 (HA-V2), but not HA-nLUC or HA-V2^{R52A}, weakened the interaction of CaM3 with CAMTA3 (Figures S7B and S7C). A similar conclusion was also drawn from *tomato yellow leaf curl China virus* (TYLCCNV) V2 experiments (Figures S7B–S7D). Thus, the V2 proteins from two different

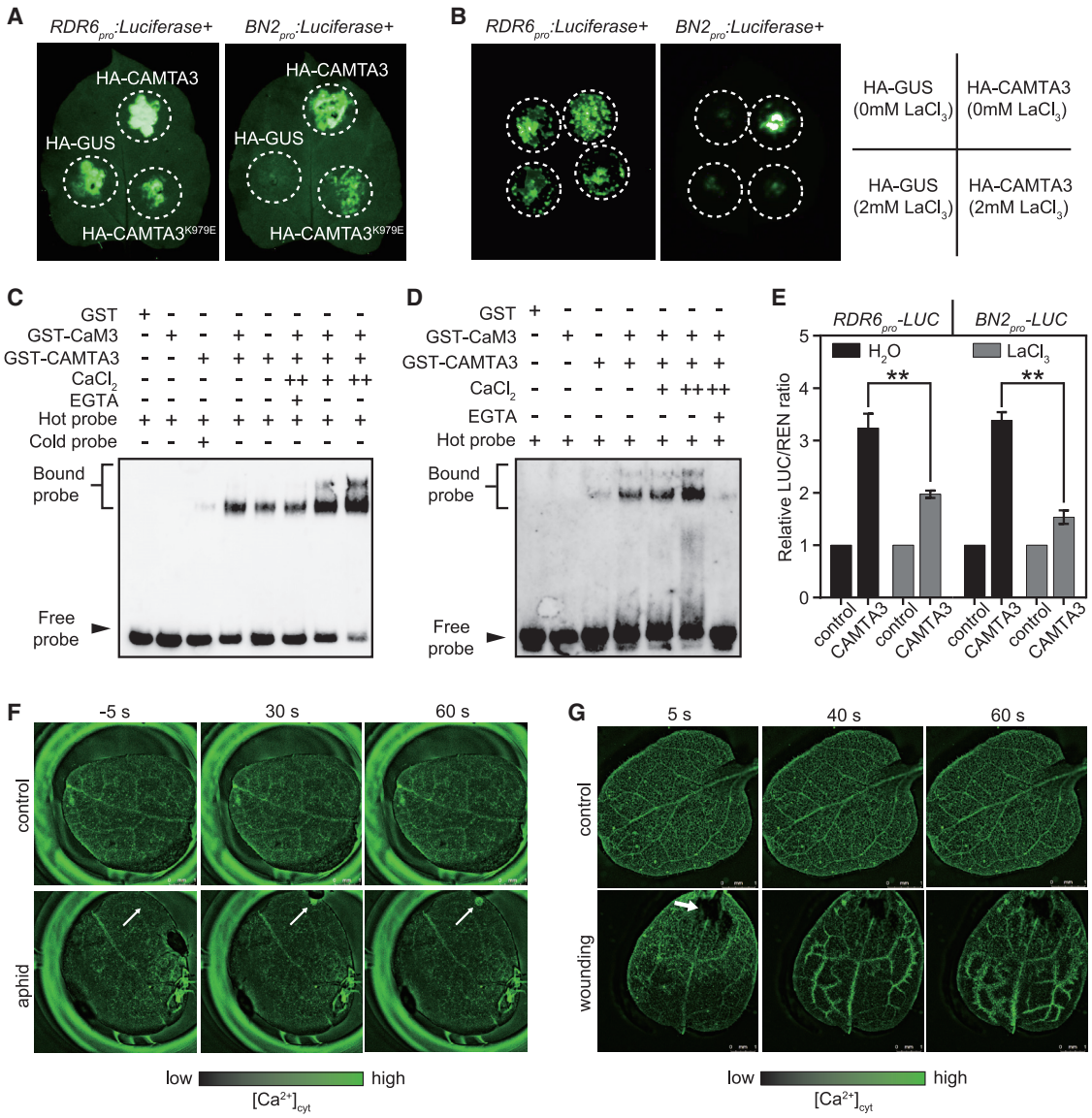

Figure 5. Calcium flux activates CAMTA3 transcription factor function

(A) Impact of K979E mutation on CAMTA3 function in luciferase report assay.

(B and E) Treatment with 2-mM $LaCl_3$ for 4 h before observation reduced CAMTA3 transcriptional upregulation of *RDR6* and *BN2* in luciferase reporter assays and *N. benthamiana* protoplast transient expression assay. The photographs were taken 30 hpi.

(C and D) EMSA showing that Ca^{2+}-coupled CaM3 interaction of CAMTA3 enhances CAMTA3 binding to promoter of *RDR6* (C) or *BN2* (D). The "+" indicates 2.5-mM $CaCl_2$, "+ +" indicates 5-mM $CaCl_2$. 10-mM EGTA was taken as treatment.

(F) An aphid feeding on the leaf caused a local $[Ca^{2+}]_{cyt}$ increase (outlined by white arrow). Ca^{2+} levels were monitored using transgenic reporter line expressing *GCaMP3*. The corresponding movie is available as Video S1.

(G) A mechanical wounding on the leaf caused a local $[Ca^{2+}]_{cyt}$ increase (outlined by white arrow). The corresponding movie is available as Video S2. Data are mean ± SD, asterisks in qRT-PCR data panels indicate a significant difference (Student's t test, *p < 0.05; **p < 0.01).

geminiviruses interfere with the interaction between CaMs and CAMTA3 to suppress plant RNAi.

Wounding-triggered Ca^{2+} flux activates antiviral RNAi in plants

During virus attack, it is yet unknown how plants sense the very first signal of virus invasion to prime the antiviral RNAi pathway. Many plant viruses enter cells through insect feeding, fungal or nematode invasion, or mechanical wounding. Wounding and insect feeding lead to Ca^{2+} flux and trigger multiple responses (Toyota et al., 2018; Vincent et al., 2017; Yan et al., 2018). In light of our results, wounding-triggered Ca^{2+} signaling could be the initial cue for priming RNAi when a virus breaks into a plant cell. This idea is supported by our results showing that CaMs and CAMTA3 positively participate in RNAi (see above). The relationship between Ca^{2+} flux and antiviral RNAi was further

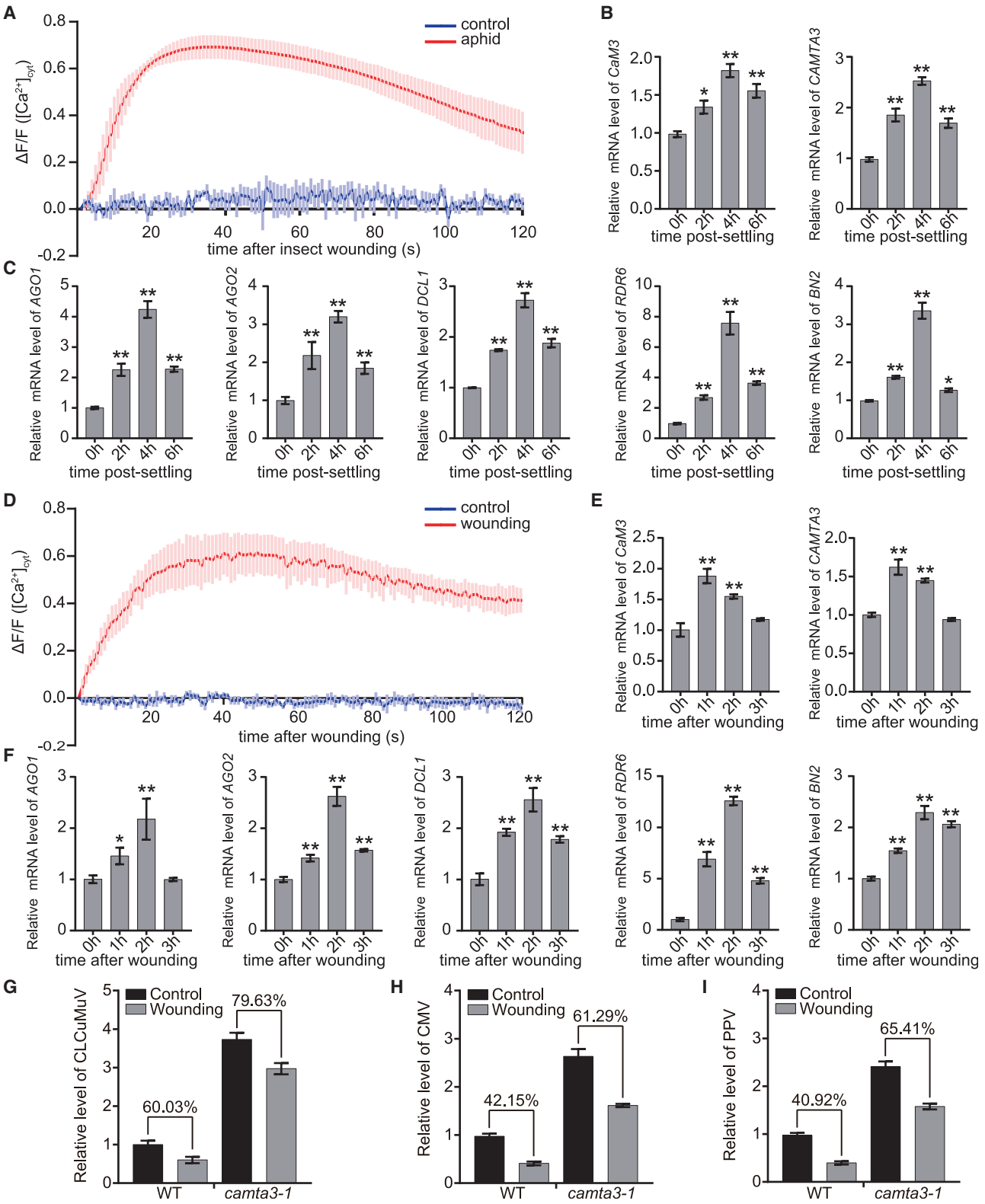

Figure 6. Wounding triggers calcium flux and bolsters RNAi in plants

(A) An aphid feeding on the leaf caused a local $[Ca^{2+}]_{cyt}$ increase. The $[Ca^{2+}]_{cyt}$ signature variation in leaf during aphid feeding. Ca^{2+} levels were monitored using transgenic reporter line expressing *GCaMP3*.

(B and C) qRT-PCR showing the relative genes induction after aphid's herbivory.

(legend continued on next page)

investigated. First, compared with CAMTA3, CAMTA3^{K979E} was reduced for CaM-binding, less transcriptional upregulation of *RDR6* and *BN2*, and less activation of RNAi (Figures 1I–1L and 5A). Second, we found that spraying plant leaves with 2-mM $LaCl_3$, an antagonist of Ca^{2+}, weakened the transcription factor activity of CAMTA3 (Figure 5B). Third, using EMSA we evaluated the effect of Ca^{2+} and CaM3 on the CAMTA3 DNA-binding activity and found that Ca^{2+}-dependent CaM3-CAMTA3 interaction enhanced CAMTA3 binding to *RDR6* or *BN2* promoter (Figures 5C and 5D). *N. benthamiana* protoplast transient expression assay displayed the same trend (Figure 5E). These data suggest that Ca^{2+}-bound CaM3 interacted with CAMTA3 to activate the CAMTA3 transcriptional function in upregulating the *RDR6* and *BN2* transcription. Fourth, we revealed that both aphid herbivory and mechanical wounding triggered Ca^{2+} signaling in *GCaMP3* overexpressing transgenic *N. benthamiana* (DeFalco et al., 2017) by inducing Ca^{2+} flux, followed by CAMTA3-dependent increases in mRNA levels for *RDR6*, *BN2*, *AGO1, AGO2*, and *DCL1* (Figures 5F, 5G, 6A–6F, 7A, and 7B; Videos S1 and S2). These observations are consistent with previous reports that different abiotic stresses trigger Ca^{2+} signaling and induce expression of *CaMs* and their downstream genes (Braam and Davis, 1990; van Der Luit et al., 1999; Yang and Poovaiah, 2000, 2002). We further evaluated the effect of wounding on viral accumulation by infecting *camta3* or wild-type *N. benthamiana* plants with PPV-GFP, CLCuMuV, or CMV-Δ2b$_{N81}$, respectively, and clamp-wounding half of them by forceps once a day on the lateral blade edge of upper systemic leaves. We examined viral accumulation in the wounded systemic leaves and systemic leaves at the same leaf position without wounding treatment and found that wounding impaired viral accumulation and *camta3* compromised the effect of wounding on viral accumulation (Figures 6G–6I). These findings suggest that *CAMTA3* is required for wounding-mediated suppression of viral accumulation. Taken together, wounding-triggered Ca^{2+} flux activates CAMTA3 function to prime RNAi for antiviral defense.

DISCUSSION

As sessile organisms, plants have evolved multilayered mechanisms to survive under diverse stresses including pathogens. It is well established that RNAi plays a crucial role in antiviral defense via the coordinated activities of RDRs, DCLs, AGOs, and RISC (Garcia-Ruiz et al., 2015; Morel et al., 2002; Qu et al., 2008; Wang et al., 2011a, 2010). RNAi can be controlled by microRNAs in a feedback manner (Allen et al., 2005; Vaucheret et al., 2004; Wu et al., 2015; Xie et al., 2003). However, two questions remain: (1) how is RNAi transcriptionally regulated to initiate, maintain, and enhance cellular RNAi machinery under normal and stress conditions and (2) what is the signal to prime RNAi at the onset of virus invasion? For most plant viruses, the first event in infection is wounding. In this work, we uncovered that when plants encounter mechanical damage or insect penetration, the wounding triggers Ca^{2+} fluxes to activate CaM-dependent CAMTA3 transcriptional function, leading to increased mRNA levels of *RDR6*, *BN2*, and several other RNAi core genes, supporting intensified antiviral RNAi response. CAMTA3 can directly bind to the *RDR6* and *BN2* promoters and activate their transcription (Figure 2). BN2 acts as a ribonuclease to degrade miRNAs, resulting in upregulation of *AGO1*, *AGO2*, and *DCL1* mRNA levels (Figures 3, S2J, and S2K). Impaired response of RNAi core genes to wounding in *camta3* or *bn2* (Figures 7A and 7B), the effect of *CAMTA3*-KD on viral infection/replication and vsiRNA accumulation in *RDR6*-KO mutant (Figures 4E–4I, S4E–S4I, and S5E–S5I), the dependence of V2-mediated RNAi suppression on the CAMTA3-CaMs interaction (Figures S6M–S6P), and the suppression effect of wounding on viral accumulation and its requirement for CAMTA3 (Figures 6G–6I) support the genetic epistasis of Ca^{2+} signaling over antiviral RNAi. These results demonstrate that Ca^{2+} signaling promotes RNAi and insect herbivory or mechanical wounding is an initial signal to prime RNAi at the onset of virus invasion (Figure 7C). Ca^{2+} and mobile RNAi signals may spread to adjacent cells to trigger intercellular and systemic $Ca^{2+} \rightarrow$RNAi signaling (Chen et al., 2018). Further, virus infection itself could result in cellular stress and alter the Ca^{2+} pools and further cause Ca^{2+} fluxes in all virus-infected cells in both local and systemic tissues (Lecourieux et al., 2006; Zhao et al., 2016) (Figure 7C). A low basal level of Ca^{2+} exists in all cells and could also contribute to basic transcription of RNAi-related genes (Figure 7C). Our findings link the Ca^{2+} signaling triggered by wounding to antiviral RNAi defense, providing insights into how plants prime RNAi on the onset and during virus invasion. Moreover, although geminiviral V2 is not predicted to have the known CaM-binding domain based on the Calmodulin Target Database (http://calcium.uhnres.utoronto.ca/ctdb/flash.htm), it suppresses antiviral RNAi by interacting with CaMs to interfere with CaM-CAMTA3 interaction and impair CAMTA3-mediated transcriptional activation of both *RDR6* and *BN2*, a distinct counter-defense strategy (Figure S7) (Li and Wang, 2019). Because of the important roles of DCL1 and AGO1 in miRNA pathway, it is possible that there also exists a positive regulation of miRNA pathway by wounding, which is involved in antiviral defense.

Tobacco *rgsCaM* has a conflicting role during virus infection (Anandalakshmi et al., 2000; Nakahara et al., 2012). In contrast, we showed that authentic CaMs promote RNAi and enhance plant defense against virus infection. On the other hand, the roles of CAMTA3 as a negative regulator of fungal and bacterial resistance in plants and as a guardee of NLRs are well established (Galon et al., 2008; Lolle et al., 2017; Rahman et al., 2016). However, *CAMTA3* is induced upon wounding and multiple physical stimuli (Yang and Poovaiah, 2002). The CAMTA3-dependent induction of RSRE suggests that CAMTA3 is a positive regulator of early stress responses (Benn et al., 2016). We now extend the functionality of CAMTA3 and CaMs to plant antiviral RNAi immunity and offers significant conceptual advance in how plants

(D) A mechanical wounding on the leaf caused a local $[Ca^{2+}]_{cyt}$ increase. The $[Ca^{2+}]_{cyt}$ signature variation in leaf mechanical wounding process. Ca^{2+} levels were monitored using transgenic reporter line expressing *GCaMP3*.
(E and F) qRT-PCR assays of genes induction after mechanical wounding.
(G–I) The effect of wounding on viral accumulation in *camta3-1* or *N. benthamiana* plants infected with CLCuMuV (G), CMV-Δ2b$_{N81}$ (H), or PPV (I). Data are mean ± SD, asterisks in qRT-PCR data panels indicate a significant difference (Student's t test, *$p < 0.05$; **$p < 0.01$).

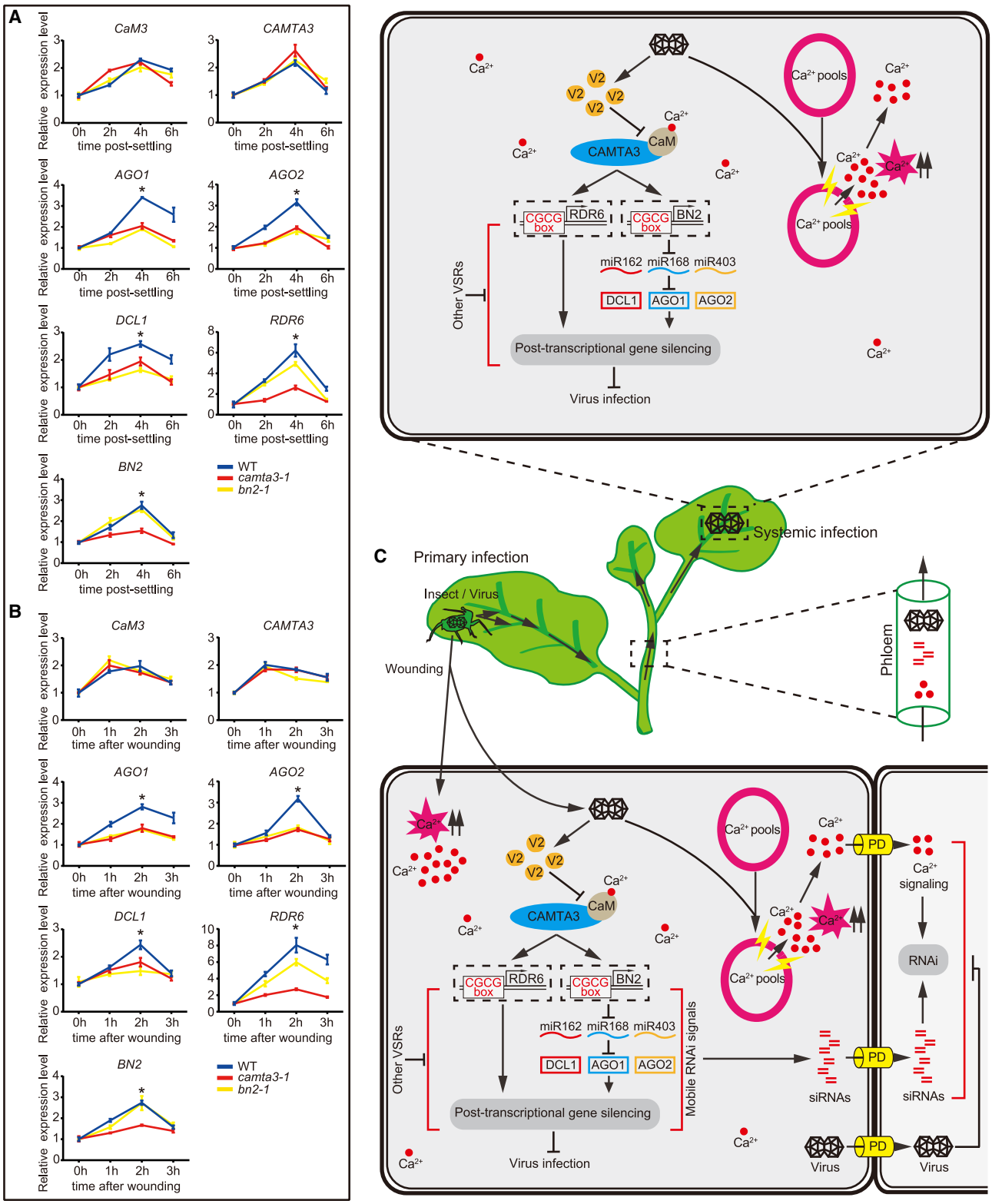

Figure 7. Effect of CAMTA3 and BN2 on wounding induced RNAi genes expression and working model

(A and B) qRT-PCR assays of gene induction after aphid's herbivory (A) or mechanical wounding (B) in camta3-1, bn2-1 and wild-type plants. Data are mean ± SD, asterisks in qRT-PCR data panels indicate a significant difference (Student's t test, *$p < 0.05$).

(legend continued on next page)

sense the initial cue of wounding to modulate RNAi in response to viral, and perhaps bacterial, fungal, or pest insect infestation during plant-pathogens arms-race. Plants recognize Ca^{2+} flux triggered by injuries to plant cells as the common molecular pattern of different viral infections to prime antiviral RNAi defense. Moreover, RNAi primed by Ca^{2+} signaling may also regulate plant development and response to abiotic stresses and other biotic stresses.

Limitations of the study

Our results suggest that Ca^{2+}-CaM-CAMTA3 signaling cascade primes RNAi defense against viruses in plants. A limitation of the study is that while we have shown that wounding-dependent calcium signaling occurs during the early stage of virus infection and CaM/CAMTA3 positively regulate antiviral silencing, it remains to be elucidated whether virus infection plays a specific, wounding-independent role in the induction of RNAi pathway genes. Additional studies will be required to understand the role of wounding-independent calcium signaling in antiviral silencing, in particular during later stages of systemic infection of plants by viruses.

STAR★METHODS

Detailed methods are provided in the online version of this paper and include the following:

- KEY RESOURCES TABLE
- RESOURCE AVAILABILITY
  - Lead contact
  - Materials availability
  - Data and code availability
- EXPERIMENTAL MODEL AND SUBJECT DETAILS
  - Plant materials and growth conditions
- METHOD DETAILS
  - Generation of transgenic plants
  - Mass spectrometry analysis
  - Yeast two hybrid (Y2H) assay
  - Yeast one hybrid (Y1H) assay
  - BiFC and LCI
  - Co-immunoprecipitation (Co-IP) assay
  - *In vitro* pull-down assay
  - Electrophoretic mobility shift assay (EMSA)
  - Quantitative real-time PCR (qRT-PCR) analysis
  - Southern blot analysis
  - Wounding
  - Real-time $[Ca^{2+}]_{cyt}$ imaging and analysis
  - Virus infection
  - Gene promoter binding site prediction
  - ChIP-qPCR analysis
  - Small RNA extraction and gel blot analysis
  - Protoplast transient expression assay
  - *In vitro* enzymatic assay for BN2
- QUANTIFICATION AND STATISTICAL ANALYSIS

SUPPLEMENTAL INFORMATION

Supplemental information can be found online at https://doi.org/10.1016/j.chom.2021.07.003.

ACKNOWLEDGMENTS

We thank Profs. Huishan Guo, Xueping Zhou, and Xianbing Wang for providing PPV, TYLCCNV, and CMV infectious clones. Funding: supported by the National Natural Science Foundation of China grants 31920103013 (Y.L.), 31530059 (Y.L.), 31421001 (Y.Q. and Y.L.) and 31872636 (Y.H.); Ministry of Science and Technology of the People's Republic of China grants 2017YFA0503401 (Y.L.) and 2017YFE0110900 (Y.H.); National Transgenic Program of China grants 2019ZX08009-003 (Y.L.), 2019ZX08005-001 (Y.L.), and 2016ZX08009001-004 (Y.H.); and National Research Development and Innovation Office of Hungary K124705 (K.F.).

AUTHOR CONTRIBUTIONS

Y.L. conceived the research; Y. Wang, Q.G., and Y.L. designed the experiments; Y. Wang, Q.G., Y. Wu, F.H., A.I., D.Z., H.L., and H.G. performed experiments with assistance from Y.L., Y.Q., K.Y., M.L., and K.F.; Y. Wang, Q.G., L.H.-B., Y.H., and Y.L. analyzed data and wrote the manuscript with contributions from all authors.

DECLARATION OF INTERESTS

The authors declare no competing interests.

Received: January 12, 2021
Revised: May 20, 2021
Accepted: July 6, 2021
Published: August 4, 2021

REFERENCES

Allen, E., Xie, Z., Gustafson, A.M., and Carrington, J.C. (2005). microRNA-directed phasing during trans-acting siRNA biogenesis in plants. Cell *121*, 207–221.

Anandalakshmi, R., Marathe, R., Ge, X., Herr, J.M., Jr., Mau, C., Mallory, A., Pruss, G., Bowman, L., and Vance, V.B. (2000). A calmodulin-related protein that suppresses posttranscriptional gene silencing in plants. Science *290*, 142–144.

Aregger, M., Borah, B.K., Seguin, J., Rajeswaran, R., Gubaeva, E.G., Zvereva, A.S., Windels, D., Vazquez, F., Blevins, T., Farinelli, L., and Pooggin, M.M. (2012). Primary and secondary siRNAs in geminivirus-induced gene silencing. PLoS Pathog *8*, e1002941.

Babu, Y.S., Bugg, C.E., and Cook, W.J. (1988). Structure of calmodulin refined at 2.2-A resolution. J. Mol. Biol. *204*, 191–204.

(C) Working model-Ca^{2+} signaling primes antiviral RNAi in plants while V2 interferes with CaM-CAMTA3 interaction to suppress RNAi. When plants encounter mechanical damage or insects feeding, the wounding rapidly triggers Ca^{2+} fluxes to activate CaM-dependent CAMTA3 transcriptional function, leading to increased mRNA levels of *RDR6*, *BN2*, and several other RNAi core genes that then intensify RNAi and defend against virus infection. CAMTA3 directly binds to *RDR6* and *BN2* promoters and activates their transcription. BN2 acts as a ribonuclease to degrade miRNAs, resulting in upregulation of *AGO1*, *AGO2*, and *DCL1* mRNA levels. Ca^{2+} and mobile RNAi signals may spread to adjacent healthy cells to trigger intercellular/systemic $Ca^{2+} \rightarrow$RNAi signaling. Virus infection could invoke the Ca^{2+} pools to cause further Ca^{2+} fluxes in infected cells of local and systemic tissues to trigger intercellular/systemic $Ca^{2+} \rightarrow$RNAi signaling. A basal level of Ca^{2+} exists in cells and can also contribute to low transcription of RNAi-related genes. Geminivirus V2 protein interferes with CaM-CAMTA3 interaction to suppress RNAi. Arrow indicates activation while the "T" sign represents attenuation or suppression. See also Figures S6 and S7.

Bai, M., Yang, G.S., Chen, W.T., Mao, Z.C., Kang, H.X., Chen, G.H., Yang, Y.H., and Xie, B.Y. (2012). Genome-wide identification of Dicer-like, Argonaute and RNA-dependent RNA polymerase gene families and their expression analyses in response to viral infection and abiotic stresses in Solanum Lycopersicum. Gene *501*, 52–62.

Benn, G., Bjornson, M., Ke, H., De Souza, A., Balmond, E.I., Shaw, J.T., and Dehesh, K. (2016). Plastidial metabolite MEcPP induces a transcriptionally centered stress-response hub via the transcription factor CAMTA3. Proc. Natl. Acad. Sci. USA *113*, 8855–8860.

Benn, G., Wang, C.Q., Hicks, D.R., Stein, J., Guthrie, C., and Dehesh, K. (2014). A key general stress response motif is regulated non-uniformly by CAMTA transcription factors. Plant J *80*, 82–92.

Bjornson, M., Benn, G., Song, X., Comai, L., Franz, A.K., Dandekar, A.M., Drakakaki, G., and Dehesh, K. (2014). Distinct roles for mitogen-activated protein kinase signaling and calmodulin-BINDING TRANSCRIPTIONAL ACTIVATOR3 in regulating the peak time and amplitude of the plant general stress response. Plant Physiol *166*, 988–996.

Braam, J., and Davis, R.W. (1990). Rain-, wind-, and touch-induced expression of calmodulin and calmodulin-related genes in Arabidopsis. Cell *60*, 357–364.

Chen, W., Zhang, X., Fan, Y., Li, B., Ryabov, E., Shi, N., Zhao, M., Yu, Z., Qin, C., Zheng, Q., et al. (2018). A genetic network for systemic RNA silencing in plants. Plant Physiol *176*, 2700–2719.

DeFalco, T.A., Marshall, C.B., Munro, K., Kang, H.G., Moeder, W., Ikura, M., Snedden, W.A., and Yoshioka, K. (2016). Multiple calmodulin-binding sites positively and negatively regulate Arabidopsis cyclic NUCLEOTIDE-GATED CHANNEL12. Plant Cell *28*, 1738–1751.

DeFalco, T.A., Toyota, M., Phan, V., Karia, P., Moeder, W., Gilroy, S., and Yoshioka, K. (2017). Using GCaMP3 to study Ca2+ signaling in Nicotiana species. Plant Cell Physiol *58*, 1173–1184.

Du, L., Ali, G.S., Simons, K.A., Hou, J., Yang, T., Reddy, A.S., and Poovaiah, B.W. (2009). Ca(2+)/calmodulin regulates salicylic-acid-mediated plant immunity. Nature *457*, 1154–1158.

Fang, X., and Qi, Y. (2016). RNAi in plants: an argonaute-centered view. Plant Cell *28*, 272–285.

Galon, Y., Finkler, A., and Fromm, H. (2010). Calcium-regulated transcription in plants. Mol. Plant *3*, 653–669.

Galon, Y., Nave, R., Boyce, J.M., Nachmias, D., Knight, M.R., and Fromm, H. (2008). Calmodulin-binding transcription activator (CAMTA) 3 mediates biotic defense responses in Arabidopsis. FEBS Lett *582*, 943–948.

Garcia-Ruiz, H., Carbonell, A., Hoyer, J.S., Fahlgren, N., Gilbert, K.B., Takeda, A., Giampetruzzi, A., Garcia Ruiz, M.T., McGinn, M.G., Lowery, N., et al. (2015). Roles and programming of Arabidopsis Argonaute proteins during Turnip mosaic virus infection. PLoS Pathog *11*, e1004755.

Hellens, R.P., Allan, A.C., Friel, E.N., Bolitho, K., Grafton, K., Templeton, M.D., Karunairetnam, S., Gleave, A.P., and Laing, W.A. (2005). Transient expression vectors for functional genomics, quantification of promoter activity and RNA silencing in plants. Plant Methods *1*, 13.

Jia, Q., Liu, N., Xie, K., Dai, Y., Han, S., Zhao, X., Qian, L., Wang, Y., Zhao, J., Gorovits, R., et al. (2016). CLCuMuB βC1 Subverts ubiquitination by Interacting with NbSKP1s to Enhance geminivirus Infection in Nicotiana benthamiana. PLoS Pathog *12*, e1005668.

Koetsier, P.A., Schorr, J., and Doerfler, W. (1993). A rapid optimized protocol for downward alkaline southern blotting of DNA. BioTechniques *15*, 260–262.

Lecourieux, D., Ranjeva, R., and Pugin, A. (2006). Calcium in plant defence-signalling pathways. New Phytol *171*, 249–269.

Li, F., and Wang, A. (2019). RNA-targeted antiviral immunity: more than just RNA silencing. Trends Microbiol *27*, 792–805.

Li, F., Zhao, N., Li, Z., Xu, X., Wang, Y., Yang, X., Liu, S.S., Wang, A., and Zhou, X. (2017). A calmodulin-like protein suppresses RNA silencing and promotes geminivirus infection by degrading SGS3 via the autophagy pathway in Nicotiana benthamiana. PLos Pathog. *13*, e1006213.

Liu, Y., Schiff, M., and Dinesh-Kumar, S.P. (2002a). Virus-induced gene silencing in tomato. Plant J *31*, 777–786.

Liu, Y., Schiff, M., Serino, G., Deng, X.W., and Dinesh-Kumar, S.P. (2002b). Role of SCF ubiquitin-ligase and the COP9 signalosome in the N gene-mediated resistance response to tobacco mosaic virus. Plant Cell *14*, 1483–1496.

Livak, K.J., and Schmittgen, T.D. (2001). Analysis of relative gene expression data using real-time quantitative PCR and the 2(-delta delta C(T)) method. Methods *25*, 402–408.

Lolle, S., Greeff, C., Petersen, K., Roux, M., Jensen, M.K., Bressendorff, S., Rodriguez, E., Sømark, K., Mundy, J., and Petersen, M. (2017). Matching NLR immune receptors to autoimmunity in camta3 mutants using antimorphic NLR alleles. Cell Host Microbe *21*, 518–529, e4.

Ludman, M., and Fátyol, K. (2019). The virological model plant, Nicotiana benthamiana expresses a single functional RDR6 homeolog. Virology *537*, 143–148.

Ma, X., Zhang, Q., Zhu, Q., Liu, W., Chen, Y., Qiu, R., Wang, B., Yang, Z., Li, H., Lin, Y., et al. (2015). A robust CRISPR/Cas9 system for convenient, high-efficiency multiplex genome editing in monocot and dicot plants. Mol. Plant *8*, 1274–1284.

Morel, J.B., Godon, C., Mourrain, P., Béclin, C., Boutet, S., Feuerbach, F., Proux, F., and Vaucheret, H. (2002). Fertile hypomorphic Argonaute (ago1) mutants impaired in post-transcriptional gene silencing and virus resistance. Plant Cell *14*, 629–639.

Nakahara, K.S., Masuta, C., Yamada, S., Shimura, H., Kashihara, Y., Wada, T.S., Meguro, A., Goto, K., Tadamura, K., Sueda, K., et al. (2012). Tobacco calmodulin-like protein provides secondary defense by binding to and directing degradation of virus RNA silencing suppressors. Proc. Natl. Acad. Sci. USA *109*, 10113–10118.

Nicaise, V. (2014). Crop immunity against viruses: outcomes and future challenges. Front. Plant Sci. *5*, 660.

Nie, H., Zhao, C., Wu, G., Wu, Y., Chen, Y., and Tang, D. (2012). SR1, a calmodulin-binding transcription factor, modulates plant defense and ethylene-induced senescence by directly regulating NDR1 and EIN3. Plant Physiol *158*, 1847–1859.

Pertermann, R., Tamilarasan, S., Gursinsky, T., Gambino, G., Schuck, J., Weinholdt, C., Lilie, H., Grosse, I., Golbik, R.P., Pantaleo, V., and Behrens, S.-E. (2018). A viral suppressor modulates the plant immune response early in infection by regulating microRNA activity. mBio *9*, e00419–18.

Qi, Y., Denli, A.M., and Hannon, G.J. (2005). Biochemical specialization within Arabidopsis RNA silencing pathways. Mol. Cell *19*, 421–428.

Qi, Y., He, X., Wang, X.J., Kohany, O., Jurka, J., and Hannon, G.J. (2006). Distinct catalytic and non-catalytic roles of ARGONAUTE4 in RNA-directed DNA methylation. Nature *443*, 1008–1012.

Qin, L., Mo, N., Muhammad, T., and Liang, Y. (2018). Genome-wide analysis of DCL, AGO, and RDR gene families in pepper (Capsicum annuum L.). Int. J. Mol. Sci. *19*, 1038.

Qu, F., Ye, X., and Morris, T.J. (2008). Arabidopsis DRB4, AGO1, AGO7, and RDR6 participate in a DCL4-initiated antiviral RNA silencing pathway negatively regulated by DCL1. Proc. Natl. Acad. Sci. USA *105*, 14732–14737.

Rahman, H., Xu, Y.P., Zhang, X.R., and Cai, X.Z. (2016). Brassica napus genome possesses extraordinary high number of CAMTA genes and CAMTA3 contributes to PAMP triggered immunity and resistance to Sclerotinia sclerotiorum. Front. Plant Sci. *7*, 581.

Ramachandran, V., and Chen, X. (2008). Degradation of microRNAs by a family of exoribonucleases in Arabidopsis. Science *321*, 1490–1492.

Ruiz, M.T., Voinnet, O., and Baulcombe, D.C. (1998). Initiation and maintenance of virus-induced gene silencing. Plant Cell *10*, 937–946.

Saleh, A., Alvarez-Venegas, R., and Avramova, Z. (2008). An efficient chromatin immunoprecipitation (ChIP) protocol for studying histone modifications in Arabidopsis plants. Nat. Protoc. *3*, 1018–1025.

Schwach, F., Vaistij, F.E., Jones, L., and Baulcombe, D.C. (2005). An RNA-dependent RNA polymerase prevents meristem invasion by potato virus X and is required for the activity but not the production of a systemic silencing signal. Plant Physiol *138*, 1842–1852.

Soosaar, J.L., Burch-Smith, T.M., and Dinesh-Kumar, S.P. (2005). Mechanisms of plant resistance to viruses. Nat. Rev. Microbiol. *3*, 789–798.

Tian, F., Yang, D.C., Meng, Y.Q., Jin, J., and Gao, G. (2020). PlantRegMap: charting functional regulatory maps in plants. Nucleic Acids Res *48*, D1104–D1113.

Toyota, M., Spencer, D., Sawai-Toyota, S., Jiaqi, W., Zhang, T., Koo, A.J., Howe, G.A., and Gilroy, S. (2018). Glutamate triggers long-distance, calcium-based plant defense signaling. Science *361*, 1112–1115.

Vaistij, F.E., and Jones, L. (2009). Compromised virus-induced gene silencing in RDR6-deficient plants. Plant Physiol *149*, 1399–1407.

van Der Luit, A.H., Olivari, C., Haley, A., Knight, M.R., and Trewavas, A.J. (1999). Distinct calcium signaling pathways regulate calmodulin gene expression in tobacco. Plant Physiol *121*, 705–714.

Vargas-Salinas, M., Medina-Hernández, D., Arcos-Ortega, G.F., Luis-Villaseñor, I.E., and Holguín-Peña, R.J. (2021). RNAi activation with homologous and heterologous sequences that induce resistance against the Begomovirus Pepper golden mosaic virus (PepGMV). 3 Biotech *11*, 114.

Vaucheret, H., Vazquez, F., Crété, P., and Bartel, D.P. (2004). The action of ARGONAUTE1 in the miRNA pathway and its regulation by the miRNA pathway are crucial for plant development. Genes Dev *18*, 1187–1197.

Vincent, T.R., Avramova, M., Canham, J., Higgins, P., Bilkey, N., Mugford, S.T., Pitino, M., Toyota, M., Gilroy, S., Miller, A.J., et al. (2017). Interplay of plasma membrane and vacuolar ion channels, together with BAK1, elicits rapid cytosolic calcium elevations in Arabidopsis during aphid feeding. Plant Cell *29*, 1460–1479.

Walley, J.W., Coughlan, S., Hudson, M.E., Covington, M.F., Kaspi, R., Banu, G., Harmer, S.L., and Dehesh, K. (2007). Mechanical stress induces biotic and abiotic stress responses via a novel cis-element. PLoS Genet *3*, 1800–1812.

Wang, L., Tsuda, K., Sato, M., Cohen, J.D., Katagiri, F., and Glazebrook, J. (2009). Arabidopsis CaM binding protein CBP60g contributes to MAMP-induced SA accumulation and is involved in disease resistance against Pseudomonas syringae. PLoS Pathog *5*, e1000301.

Wang, W., Ye, R., Xin, Y., Fang, X., Li, C., Shi, H., Zhou, X., and Qi, Y. (2011a). An importin beta protein negatively regulates microRNA activity in Arabidopsis. Plant Cell *23*, 3565–3576.

Wang, X.B., Jovel, J., Udomporn, P., Wang, Y., Wu, Q., Li, W.X., Gasciolli, V., Vaucheret, H., and Ding, S.W. (2011b). The 21-nucleotide, but not 22-nucleotide, viral secondary small interfering RNAs direct potent antiviral defense by two cooperative argonautes in Arabidopsis thaliana. Plant Cell *23*, 1625–1638.

Wang, X.B., Wu, Q., Ito, T., Cillo, F., Li, W.X., Chen, X., Yu, J.L., and Ding, S.W. (2010). RNAi-mediated viral immunity requires amplification of virus-derived siRNAs in Arabidopsis thaliana. Proc. Natl. Acad. Sci. USA *107*, 484–489.

Wang, Y., Wu, Y., Gong, Q., Ismayil, A., Yuan, Y., Lian, B., Jia, Q., Han, M., Deng, H., Hong, Y., et al. (2019). Geminiviral V2 protein suppresses transcriptional gene silencing through interaction with AGO4. J. Virol. *93*, e01675–18.

Wilson, R.C., and Doudna, J.A. (2013). Molecular mechanisms of RNA interference. Annu. Rev. Biophys. *42*, 217–239.

Wu, J., Yang, Z., Wang, Y., Zheng, L., Ye, R., Ji, Y., Zhao, S., Ji, S., Liu, R., Xu, L., et al. (2015). Viral-inducible Argonaute18 confers broad-spectrum virus resistance in rice by sequestering a host microRNA. eLife *4*, e05733.

Xie, Z., Kasschau, K.D., and Carrington, J.C. (2003). Negative feedback regulation of Dicer-Like1 in Arabidopsis by microRNA-guided mRNA degradation. Curr. Biol. *13*, 784–789.

Yamaguchi, N., Winter, C.M., Wu, M.F., Kwon, C.S., William, D.A., and Wagner, D. (2014). PROTOCOLS: chromatin immunoprecipitation from Arabidopsis tissues. Arabidopsis Book *12*, e0170.

Yan, C., Fan, M., Yang, M., Zhao, J., Zhang, W., Su, Y., Xiao, L., Deng, H., and Xie, D. (2018). Injury activates Ca(2+)/calmodulin-dependent phosphorylation of JAV1-JAZ8-WRKY51 complex for jasmonate biosynthesis. Mol. Cell *70*, 136–149, e7.

Yang, T., and Poovaiah, B.W. (2000). An early ethylene up-regulated gene encoding a calmodulin-binding protein involved in plant senescence and death. J. Biol. Chem. *275*, 38467–38473.

Yang, T., and Poovaiah, B.W. (2002). A calmodulin-binding/CGCG box DNA-binding protein family involved in multiple signaling pathways in plants. J. Biol. Chem. *277*, 45049–45058.

Yang, Z., Huang, Y., Yang, J., Yao, S., Zhao, K., Wang, D., Qin, Q., Bian, Z., Li, Y., Lan, Y., et al. (2020). Jasmonate signaling enhances RNA silencing and antiviral defense in rice. Cell Host Microbe *28*, 89–103, e8.

Ying, X.B., Dong, L., Zhu, H., Duan, C.G., Du, Q.S., Lv, D.Q., Fang, Y.Y., Garcia, J.A., Fang, R.X., and Guo, H.S. (2010). RNA-dependent RNA polymerase 1 from Nicotiana tabacum suppresses RNA silencing and enhances viral infection in Nicotiana benthamiana. Plant Cell *22*, 1358–1372.

Yoo, S.D., Cho, Y.H., and Sheen, J. (2007). Arabidopsis mesophyll protoplasts: a versatile cell system for transient gene expression analysis. Nat. Protoc. *2*, 1565–1572.

Zhao, J., Zhang, X., Hong, Y., and Liu, Y. (2016). Chloroplast in plant-virus interaction. Front. Microbiol. *7*, 1565.

STAR★METHODS

KEY RESOURCES TABLE

REAGENT or RESOURCE	SOURCE	IDENTIFIER
Antibodies		
Rat monoclonal anti-GFP	ChromoTek	Cat#3h9-100; RRID:AB_10773374
Goat anti-Rat	ABclonal	Cat# AS028; RRID:AB_2769855
Rabbit polyclonal anti-GFP	Abcam	Cat# ab290; RRID:AB_303395
Mouse monoclonal anti-HA	CST	Cat#2999S; RRID:AB_1264166
Mouse monoclonal anti-MYC	Abmart	Cat#M20002M; RRID:AB_2861172
Mouse monoclonal anti-GST	ABclonal	Cat#AE001; RRID: AB_2770403
Mouse monoclonal anti-His	Abcam	Cat# ab18184; RRID:AB_444306
Goat anti-Rabbit	Abcam	Cat# ab205718; RRID:AB_2819160
Anti-MBP monoclonal antibody	New England Biolabs	Cat#E8038; RRID:AB_1559738
Bacterial and virus strains		
Escherichia coli strain BL21 (DE3)	ZOMANBIO	Cat# ZC121-1
Saccharomyces cerevisiae strain AH109	Clontech	N/A
Saccharomyces cerevisiae strain Y187	Clontech	Cat#630457
Agrobacterium tumefaciens strain GV2260	ZOMANBIO	Cat# ZC1411
Escherichia coli strain DH5α	ZOMANBIO	Cat#ZC101
Cotton leaf curl Multan virus	Wang et al., 2019	N/A
Tomato yellow leaf curl China virus	Li et al., 2017	N/A
Plum pox virus	Ying et al., 2010	N/A
Cucumber mosaic virus	Wang et al., 2011b	N/A
Tobacco rattle virus	Liu et al., 2002b	N/A
Chemicals, peptides, and recombinant proteins		
$LaCl_3$	Sigma-Aldrich	Cat#449830-25G
EGTA	Sigma-Aldrich	Cat#E4378
$CaCl_2$	Sigma-Aldrich	Cat#C3306
Complete protease inhibitor cocktail	Roche	Cat#4693116001
Glutathione Sepharose 4B	GE Healthcare	Cat#17-0756-01
Ni-NTA Agrose	Qiagen	Cat#30210
Amylose Resin	New England Biolabs	Cat#E8021L
RNasin Ribonuclease Inhibitor	Promega	Cat#N2111S
Alkaline Phosphatase, Calf Intestinal (CIP)	Takara	Cat#2250B
Critical commercial assays		
Dual-Luciferase Reporter Assay System	Promega	Cat#E1910
Chemiluminescent EMSA Kit	Beyotime	Cat#GS009
Hieff® qPCR SYBR® Green Master Mix	YEASEN	Cat#11201ES08
RiboMAX™ Large Scale RNA Production Systems	Promega	Cat#P1300
TransScript One-Step gDNA Removal and cDNA Synthesis SuperMix	Transgen Biotech	Cat#AT311-02
SimpleChIP(R) Plus Kit (Magnetic Bead)	CST	Cat#9005S
miRcute miRNA First-Strand cDNA Synthesis Kit	TIANGEN	Cat#KR201
miRcute miRNA qPCR detection Kit (SYBR)	TIANGEN	Cat#FP401
Biotin DecaLabel DNA Labeling Kit	Fermentas	Cat#K0651

(*Continued on next page*)

Continued		
REAGENT or RESOURCE	SOURCE	IDENTIFIER
BcaBEST™ Labeling Kit	TaKaRa	Cat#6046
North2South Chemiluminescent Hybridization and Detection Kit	Pierce	Cat#17097
Deposited data		
SRA	sRNA-seq of *Nicotiana benthamiana*	PRJNA611704
SRA	sRNA-seq of *bn2-1* transgenic plants	PRJNA611711
Raw data of EMSA, western blots, northern blots and southern blots	Mendeley Data	https://data.mendeley.com/datasets/k5r6z5zkpk/draft?a=379ee2d9-9261-4541-8fd1-15ef39af9af5
Experimental models: Organisms/strains		
Nicotiana: 16c	Ruiz et al., 1998	N/A
Nicotiana: *35S:MYC-GUS*	This paper	N/A
Nicotiana: *35S:MYC-CaM3*	This paper	N/A
Nicotiana: *camta3-1* (WT background)	This paper	N/A
Nicotiana: *camta3-2* (WT background)	This paper	N/A
Nicotiana: *camta3-3* (16c background)	This paper	N/A
Nicotiana: *bn2-1* (WT background)	This paper	N/A
Nicotiana: *bn2-2* (WT background)	This paper	N/A
Nicotiana: *35S:GCaMP3*	DeFalco et al., 2017	N/A
Nicotiana: *rdr6* (WT background)	Ludman and Fátyol, 2019	N/A
Nicotiana: RDR6i (WT background)	Schwach et al., 2005	N/A
Oligonucleotides		
See Table S2		N/A
Recombinant DNA		
HA/GFP/GST/MBP/BD-V2	This paper	N/A
V2-nYFP/nLUC	This paper	N/A
HA/GFP/GST/MBP/BD-V2^{R52A}	This paper	N/A
V2 ^{R52A}-nYFP	This paper	N/A
HA/MBP-TYLCCNV V2	This paper	N/A
cLUC/AD/cYFP/nYFP/MYC/His-NbCaM3	This paper	N/A
cYFP/HA/GST/ pGADT7-NbCAMTA3	This paper	N/A
pGreenII 62-SK-NbCAMTA3	This paper	N/A
MYC/cLUC -NbCaM1	This paper	N/A
MYC/cLUC -NbCaM6	This paper	N/A
GST/cYFP-CaMBD	This paper	N/A
cYFP/GST/HA-NbCAMTA3^{K979E}	This paper	N/A
RDR6pro/RDR6Mpro-Luciferase	This paper	N/A
pHIS2-*RDR6pro/RDR6Mpro*	This paper	N/A
pGreen II 800-RDR6pro/RDR6Mpro	This paper	N/A
BN2pro/BN2Mpro-Luciferase	This paper	N/A
pHIS2-*BN2pro/BN2Mpro*	This paper	N/A
pGreen II 800-BN2pro/BN2Mpro	This paper	N/A
HA/GST-BN2 (BN2M)	This paper	N/A
35S:Pri-miR162	This paper	N/A
35S:Pri-miR168	This paper	N/A
35S:Pri-miR403	This paper	N/A
35S:GFP	Ying et al., 2010	N/A
MBP-GFP	This paper	N/A
T7Pro:Pri-miR168	This paper	N/A
T7Pro:ACTIN 2 partial	This paper	N/A

(*Continued on next page*)

Continued

REAGENT or RESOURCE	SOURCE	IDENTIFIER
βM2-NbPDS	Jia et al., 2016	N/A
βM2-NbCaM3	This paper	N/A
CMV-Δ2b$_{N81}$	This paper	N/A
CLCuMuV-V2 ^{R52A}	This paper	N/A
TRV-NbCaM3	This paper	N/A
TRV-CAMTA3	This paper	N/A
TRV-NbPDS	Liu et al., 2002a	N/A
Software and algorithms		
ClusterX	Version 2	www.clustal.org
Prism7	GraphPad	www.graphpad.com
LAS X	Leica	www.leica-microsystems.com
ZEN	Zeiss	www.zeiss.com

RESOURCE AVAILABILITY

Lead contact

Further information and request for resources and reagents should be directed to and will be fulfilled by the Lead Contact, Yule Liu (yuleliu@mail.tsinghua.edu.cn).

Materials availability

All unique/stable reagents generated in this study are available from the Lead Contact with a completed Materials Transfer Agreement.

Data and code availability

All data and materials needed to replicate the work are available. Accession numbers: Sequence data from this article can be found in the GenBank/EMBL databases under the following accession numbers: *CaM1* (MN746380); *CaM3* (MN746379); *CaM6* (MN746381); *CAMTA3* (MN746383); *BN2* (MN746382); CLCuMuV (GQ924756). WT and *bn2* sRNA sequencing data have been deposited in National Center for Biotechnology Information (NCBI) under Bioproject PRJNA611704 and PRJNA611711. Original data have been deposited to Mendeley Data: https://data.mendeley.com/datasets/k5r6z5zkpk/draft?a=379ee2d9-9261-4541-8fd1-15ef39af9af5.

EXPERIMENTAL MODEL AND SUBJECT DETAILS

Plant materials and growth conditions

16c lines were GFP-expressing *Nicotiana benthamiana* plants as described (Ruiz et al., 1998). *MYC-CaM3* or *MYC-GUS* transgenic lines are *N. benthamiana* lines overexpressing *CaM3* or *GUS* with N-terminal fusion to a MYC tag. The *camta3-1* and *camta3-2* were *CAMTA3*-edited KO mutant *N. benthamiana* lines, and *camta3-3* was *CAMTA3*-edited KO mutant line with 16c background. The *bn2-1* and *bn2-2* were *BN2*-edited KO mutant *N. benthamiana* lines. The CRISPR/Cas9 plants construction was described in generation of transgenic plants section performed as (Ma et al., 2015). *RDR6*-RNAi line (*rdr6i*) was kindly provided by Baulcombe's group (Schwach et al., 2005). The *RDR6*-KO (*rdr6*) plants were described (Ludman and Fátyol, 2019). All seeds were surface-sterilized and plated on MS medium (Murashige and Skoog medium, Sigma-Aldrich), and grown at 26°C with a 16 h/8 h light/dark photoperiod. For adult plants, 10-day-old seedlings were planted in soil and grown under the same conditions. For insect and mechanical wounding, plants were grown for 20 days in soil. For virus infection, plants were grown in soil for 3-4 weeks.

METHOD DETAILS

Generation of transgenic plants

The full-length *CaM3* or *GUS* gene was PCR-amplified and cloned into pCambia1300-based binary vector under the control of CaMV 35S promoter by ligation-independent cloning assay to generate the MYC-tagged construct (*35S:MYC-CaM3* or *35S:MYC-GUS*). All constructs were verified by sequencing and transformed into *N. benthamiana* leaf discs by *Agrobacterium*. Leaf discs were plated on MS medium with 0.1 mg/mL NAA (Solarbio, N8010), 1.0 mg/mL 6-BA (Solarbio, IB0100) and 0.025 mg/mL Hygromycin B (Merck millipore, 400052). The T2 generation transgenic lines of *35S:MYC-CAM3* or *35S:MYC-GUS* were identified by western blot and qRT-PCR, and then used for virus infection. The *camta3* and *bn2* Cas9-edited mutant lines were generated as described (Ma et al., 2015). Briefly, the fragment containing two sgRNAs (CAMTA3_LacZ/AtU3d-sgRNA1-At3b-sgRNA2) or single sgRNA (BN2_LacZ/AtU3d-sgRNA) were cloned into pYLCRISPR/Cas9-DH respectively to generate pYLCRISPR/Cas9-DH-CAMTA3 and pYLCRISPR/Cas9-DH-BN2.

The sgRNA sequences are listed in Table S2. These two CRISPR constructs were transformed into wild-type or 16c *N. benthamiana* leaf discs by *Agrobacterium*. The *camta3-1/3* transgenic lines were edited at Target 1 and *camta3-2* transgenic line was edited at Target 2. The editing target sites were characterized by PCR sequencing to select homozygous transgenic lines. The progenies of homozygous *camta3* and *bn2* lines showed no marked developmental phenotype and were used as experimental materials.

Mass spectrometry analysis

Agrobacterium strains containing 35S:MYC-CaM3 or 35S:MYC-GUS control construct were infiltrated into 4-week-old *N. benthamiana* leaves respectively. At 48 h post agroinfiltration, the leaves were collected and ground into fine powder in liquid nitrogen. Total proteins were subsequently extracted in Co-IP buffer [50 mM Tris-HCl, pH 7.5, 150 mM NaCl, 10% glycerol, 0.5 mM EDTA, 0.5% NP-40, and freshly added 5 mM DTT, 1 mM PMSF and 1 X protease inhibitor cocktail (Roche)]. After incubation on ice for 40 min, the extracts were centrifuged twice at 12,000 g for 20 min at 4°C. Protein extracts were immunoprecipitated by MYC-Trap beads (Abmart, Cat#M20012L). The mixture was incubated for 3 h at 4°C. The precipitated samples were washed 5 times with Co-IP buffer and then immunoprecipites were denatured using 2 X protein loading buffer contains β-mercaptoethanol at 95 °C for 10 min and separated by 10% SDS-PAGE. The gel was silver stained and gel-embedded protein samples were digested and LC-MS/MS analyzed.

Yeast two hybrid (Y2H) assay

For the Y2H assay, *V2*, *V2*^{R52A} and *Calmodulin3* were cloned into pGBKT7 (BD) or pGADT7 (AD) vectors by ligation-independent cloning assay. Y2H assays were performed as described (Wang et al., 2019). The *SKP1* and *βC1* were cloned into AD and BD as positive controls (Jia et al., 2016). Primers used for the vector construction are presented in Table S2. The yeast strain AH109 (Clontech) co-transformed with identical combinations were spotted on selective media (minus (-) His, Leu and Trp) contained 2 mM 3-amino-1, 2, 4-triazole (3-AT). Images were taken at 3 days after incubation at 28°C. Experiments were repeated at least three times. The Y2H prey library containing tomato cDNA (Liu et al., 2002b) was used to screen V2-interacting proteins. The Y2H screening assays were performed as described (Liu et al., 2002b).

Yeast one hybrid (Y1H) assay

The full-length cDNA sequences of *CAMTA3* was amplified and fused in frame with the GAL4 activation domain of pGADT7-Rec2 (Clontech) by ligation-independent cloning assay. The fusion construct was co-transformed with the reporter vector (pHIS2-cis/promoter of *RDR6*/ *RDR6M* or *BN2*/ *BN2M*) into Y187 yeast cells (Clontech) by ligation-independent cloning assay. The empty vector pGADT7-Rec2 and the pHIS2-cis/35S promoter were transformed as negative controls. Co-transformed yeast strain Y187 were spotted on selective media (minus (-) His, Leu and Trp) contained 0.5 or 2 mM 3-AT. Images were taken at 3 days after incubation at 28°C. Y1H experiments were repeated at least three times.

BiFC and LCI

Bimolecular fluorescence complementation (BiFC) and firefly luciferase complementation imaging (LCI) methods were described as (Wang et al., 2019). For BiFC assays, the full-length coding sequences of *CaM3*, *CAMTA3*, CLCuMuV *V2* and CLCuMuV *V2*^{R52A} were cloned into the binary nYFP or cYFP vector by ligation-independent cloning assay. Primer pairs for constructs are listed in Table S2. These constructs were transformed into *Agrobacterium* strain GV2260 and transiently co-expressed with indicated combinations in *N. benthamiana* leaves. The YFP fluorescence signal for each combination was detected after 48 h infiltration by an inverted confocal microscope (Zeiss LSM780). The expression level of nYFP-CaM3 and cYFP-CAMTA3 fusion proteins in tobacco leaf was detected by western blotting using rabbit polyclonal anti-GFP antibody (Abcam, Cat# ab290) and Goat anti-Rabbit antibody (Abcam, Cat# ab205718). For LCI assays, the full-length coding sequences of *V2* and *CaMs* were cloned into nLUC vector and cLUC vector by ligation-independent cloning assay. These constructs were then transformed into *GV2260* and co-expressed in *N. benthamiana* leaves for 48 h. The luciferase substrate (luciferin) was sprayed onto the surface of leaves and images were taken using a low-light cooled imaging apparatus (Andor iXon). All of these experiments were independently repeated at least 3 times and produced similar results.

Co-immunoprecipitation (Co-IP) assay

Agrobacterium strains constructs were mixed and co-infiltrated into 4-week-old *N. benthamiana* leaves. 48 hours post agroinfiltration, the leaves were collected for protein extraction. Protein extracts were immunoprecipitated by MYC-Trap beads (Abmart, Cat#M20012L) in Co-IP buffer. The mixture was incubated for 3 h at 4°C. The precipitated samples were washed 5 times with Co-IP buffer and then eluted by the addition of SDS protein loading buffer. After boiling for 10 min, the clear supernatant was separated in a 10% SDS-PAGE gel followed by immunoblot analysis. Anti-HA (CST, Cat#2999S), anti-MYC (Abmart, Cat#M20002M), anti-GFP (ChromoTek, Cat#3h9-100) or anti-Rat (ABclonal, Cat#AS028) antibodies were used for immunoblot analysis. All antibodies were used at a 1:3000 dilution. StarSignal Chemiluminescent Assay Kit (GeneStar, Cat#E171-01) was used for signal detection following the manufacturer's protocol. These experiments were repeated three times and generated similar results.

In vitro pull-down assay

$V2^{R52A}$ site-directed mutagenesis was made by pClone007 Vector Kit (Tsingke). We expressed histidine-tagged CaM3 (His-CaM3), GST, GST-CaMBD, GST-$CAMTA3^{K979E}$, GST-V2, GST-$V2^{R52A}$, myelin basic protein (MBP)-GFP, MBP-V2, MBP-$V2^{R52A}$ and MBP-V2 (TYLCCNV) in *E. coli* strain BL21 (DE3) (ZOMANBIO) by inducing with 0.3 mM isopropyl b-D-thiogalactoside (IPTG) for 16 h at 16°C. *E. coli* cells were collected and sonicated in ice-cold lysis buffer (100 mM NaCl, 50 mM Tric-HCl, pH 8.0) for protein purification. GST-tagged recombinant proteins were purified by Glutathione Sepharose 4B (GE Healthcare) affinity chromatography and eluted by 10 mM GSH. MBP-tagged recombinant proteins were purified by Amylose Resin (New England Biolabs) and eluted by 20 mM maltose. His-CaM3 was purified by Ni-NTA Agarose (Qiagen) affinity chromatography and eluted by imidazole. The recombinant proteins in elution buffer were then purified by size exclusion chromatography (Superdex 200 10/300, GE Healthcare). The purified proteins were used to perform pull-down assay. For analysis of the effect of V2 proteins on CaM-CaMBD interaction, purified His-CaMs were captured with Ni-NTA, and then incubated with GST-CaMBD along with an increasing gradient of MBP-GFP, MBP-$V2^{R52A}$, MBP-V2 or MBP-V2 (TYLCCNV) at 4°C for 1 h. For analysis of Ca^{2+} effect on CaM3-CAMTA3 interaction *in vitro*, His-CaM3 were purified from *E. coli* lysate by Ni-NTA Agarose (Qiagen) affinity chromatography and eluted by imidazole. The elution buffer containing His-CaM3 was divided into three parts. Two parts were adjusted to have 10 mM EGTA and 5 mM $CaCl_2$ respectively and the third part was used as control, incubated at 4°C for 1 h, followed by size exclusion chromatography (Superdex 200 10/300, GE Healthcare) to remove the EGTA or $CaCl_2$ and collect the purified protein respectively. Purified His-CaM3 was then captured with Ni-NTA again. The Ni-NTA was washed with lysis buffer five times, and then incubated with purified GST or GST-CAMTA3 at 4°C for 1 h. The precipitated prey proteins were released by boiling in SDS sample buffer for 10 min and checked by immunoblot analysis using anti-GST (ABclonal, Cat#AE001), anti-His (Abcam, Cat#ab18184) or Anti-MBP (New England Biolabs, Cat#E8038) antibodies.

Electrophoretic mobility shift assay (EMSA)

GST, GST-CaM3 and GST-CAMTA3 proteins were purified by Glutathione Sepharose 4B (GE Healthcare) affinity chromatography and eluted by 10 mM GSH followed by size exclusion chromatography (Superdex 200 10/300, GE Healthcare). Oligonucleotide probes were synthesized and labeled with the biotin by RUIBIO Technology Company. EMSA was performed using the Chemiluminescent EMSA Kit (Beyotime, GS009). Briefly, 10 μg of the indicated protein was incubated with 20 fmol biotinlabeled oligos in binding buffer (Beyotime, GS009) for 10 min at room temperature. For competitive EMSA, 4 pmol of unlabeled oligos were added into the reaction mixture at 20 min prior to the addition of a constant amount of the labeled positive oligos. For testing Ca^{2+}-CaM effect on CAMTA3 binding of *RDR6* and *BN2* promoter, reaction mixtures were adjusted to have 2.5 mM/5 mM $CaCl_2$ (indicated as "+"/"+ +") or 10 mM EGTA respectively. The reaction mixtures were resolved on 1 mm-thick 5% non-denaturing polyacrylamide gels and transferred to Hybond TM-N^+ membranes (Beyotime, FFN13). The DNA oligomers were UV crosslinked to the membrane and the labeled probes were detected by the LightShift Chemiluminescent EMSA Kit (Beyotime, GS009). Experiments were repeated at least three times.

Quantitative real-time PCR (qRT-PCR) analysis

Total RNA was extracted with TransZol reagent (Transgen Biotech) and 5 μg of RNA was reverse-transcribed into cDNA with TransScript One-Step gDNA Removal and cDNA Synthesis SuperMix (Transgen Biotech, Cat#AU311-02) according to the manufacturer's instructions. Total DNA was isolated from virus-infected *N. benthamiana* leaves as described (Jia et al., 2016). 50 ng/μL DNA was used as template to perform qRT-PCR for analysis of CLCuMuV virus amount. qRT-PCR was performed in a BIORAD qPCR instrument using Hieff® qPCR SYBR® Green Master Mix (YEASEN, Cat#11201ES08). Data was normalized to *ACTIN* expression by the cycle threshold (CT) $2\text{-}\Delta\Delta^{CT}$ method, as described (Livak and Schmittgen, 2001) and analyzed by Prism7 software (Graphpad). MiRcute miRNA First-Strand cDNA Synthesis Kit and miRcute miRNA qPCR detection Kit (TIANGEN, Cat#KR211, Cat #FP401) were used for analysis of plant miRNAs. All experiments were repeated at least three times. Primers used in this study are in Table S2. Data are mean ± s.d., asterisks in qRT-PCR data panels indicate a significant difference (Student's t-test, *P<0.05; **P<0.01).

Southern blot analysis

3 μg DNA was separated on a 20cm x 20cm x 0.8cm 1% agarose gel by electrophoresis at 100 V/cm for 100 min. Downward alkaline gel blotting was then performed using Immobilon-NY^+ Charged Nylon (Merck Millipore) for 10 h as described (Koetsier et al., 1993). After transmembrane, Cross-link DNA onto nylon using UV cross linker. The *V1* DNA fragment was labelled by Biotin DecaLabel DNA Labeling Kit (Pierce, Cat#K0651) and used as probes for DNA hybridization. The primer pairs for *V1* sequence are in Table S2. Hybridization and DNA membrane detection were performed by North2South Chemiluminescent Hybridization and Detection Kit (Pierce, Cat#17097). Experiments were repeated at least three times.

Wounding

Many plant viruses enter cells associated with insect feeding, fungal or nematode invasion, or mechanical wounding. Wounding and insect feeding lead to Ca^{2+} flux and trigger multiple responses. To analyze the effect of wounding on mRNA levels of *CaM3*, *CAMTA3* and other genes, leaves of 20-days-old *N. benthamiana*, *camta3-1* or *bn2-1* plants in soil were first detached, cut in half along the midrib and cultivated on MS plate for 24 h before wounding treatment. For mechanical wounding, the half leaf was clamp-wounded once by a forcep. The leaf was sampled at different time points after wounding along with another half leaf without wounding as a control. For insect wounding, 5 aphids were placed on half of leaves and samples were taken at different time points all along

with aphids on the surface of leaves. Another half of leaves without aphid treatment was sampled at the same time as controls.

Real-time $[Ca^{2+}]_{cyt}$ imaging and analysis

N. benthamiana plants expressing the GFP-based Ca^{2+} indicator, GCaMP3, were imaged with a motorized fluorescence stereo microscope (M205FCA, Leica) equipped with a 1× objective lens (NA = 0.17, Leica) and a sCMOS camera (Leica). The green fluorescent signal passing through the ET GFP - M205FA Filter was acquired with the sCMOS camera using LAS X software (installed with THUNDER Imager Model Organism). The green fluorescent signal in figures were analyzed by LAS X software. To calculate the fractional fluorescence changes (ΔF/F), the equation ΔF/F = (F - F0)/F0 was used, where F0 denotes the average baseline fluorescence determined by the average of F over the first 5 frames of the recording before the wounding treatment (Toyota et al., 2018).

Virus infection

PPV-GFP is provided as a kind gift from Prof. Huishan Guo. CMV-Fny infectious clone was kindly provided by Prof. Xianbing Wang. CMV-Δ2b_{N81} (retained N-terminal 81 amino acids of 2b) was generated by deleting partial sequence of CMV-2b of CMV-Fny infectious clone. For testing the effect of *CAMTA3* and *BN2* on virus infection, *camta3-1, bn2-1* and *N. benthamiana* plants were grown in soil for 3-4 weeks and infected with CLCuMuV, PPV-GFP or CMV-Δ2b_{N81} through agro-infiltration. Viral symptoms were photographed at 16 days post inoculation (dpi) for CLCuMuV, 7 dpi for PPV-GFP or 8 dpi for CMV-Δ2b_{N81} respectively. For performing virus infection in silenced plants, 20-day-old plants were first agro-infiltrated with TRV-*CAMTA3* or TRV, and the upper leaves were then infected with CLCuMuV, PPV-GFP or CMV-Δ2b_{N81} at 14 days after VIGS treatment. Viral symptoms were photographically recorded at 16 dpi for CLCuMuV, 8 dpi for PPV-GFP or 11 dpi for CMV-Δ2b_{N81} respectively. For analysis of effect of *CaM3* silencing on virus infection, 3 weeks old *N. benthamiana* was agro-inoculated with CLCuMuV along with βM2-*nLUC* or βM2-*CaM3*. Photographs of viral symptoms were taken at 16 dpi. For analysis of effect of *CaM3* overexpression on virus infection, 3-week-old *MYC-CaM* and *MYC-GUS* transgenic lines were infected with CLCuMuV. Photographs of viral symptoms were taken at 20 dpi. For analysis of geminivirus-induced gene silencing, 3-week-old *camta3-1*, *rdr6i* or wild-type *N. benthamiana* plants were agroinoculated with CLCuMuV and βM2-*PDS*, photographs were taken at 20 dpi. For testing the effect of *RDR6* on TRV-mediated VIGS, 3-week-old wild-type or *rdr6i N. benthamiana* plants were agroinfiltrated with TRV-*NbPDS* and photographs were taken at 16 dpi. For mutant virus assays, 3-week-old plants were agroinfiltrated with CLCuMuV or mutant virus CLCuMuV-$V2^{R52A}$ and samples were collected for southern blot at 16 dpi. For analysis of *CAMTA3* effect on mutant virus infection, *camta3-1* or *N. benthamiana* plants were agroinfiltrated with CLCuMuV or CLCuMuV-$V2^{R52A}$ and upper systemic leaves were collected at 6 dpi. For analysis of wounding effect on viral accumulation, 3-week-old wild-type or *camta3-1* plants were infected with CLCuMuV, PPV-GFP or CMV-Δ2b_{N81}. These infected plants were then divided into the test (wounding) and control (without wounding) group. Plants in the test group were clamp-wounded by forceps on upper systemic leaves once a day up to sample collection, the wounded systemic leaves were collected at 6 dpi (PPV-GFP and CMV-Δ2b_{N81}) or 14 dpi (CLCuMuV) for the analysis of viral accumulation against the leaves of plants at the same leaf position in the control group.

Gene promoter binding site prediction

The 2000 base pairs (bp) of putative promoter sequences of candidate *N. benthamiana* genes were downloaded from https://solgenomics.net/. The PlantRegMap program (http://plantregmap.gao-lab.org) was applied for scanning the candidate transcription factors of target promoters as described (Tian et al., 2020).

ChIP-qPCR analysis

ChIP-qPCR (Chromatin immunoprecipitation-quantitative) was performed following a published protocol with minor modifications (Saleh et al., 2008). *N. benthamiana* leaves over-expressing *HA-CAMTA3* or *HA-nLUC* were collected and chromatin was isolated from 2 g of frozen leaf tissue and sonicated with a Bioruptor sonicator for 6 min. Immunoprecipitation was performed by incubating chromatin with 50 μL anti-HA magnetic agarose bead for 3 h at 4°C. SimpleChIP(R) Plus Kit (CST, Cat#9005S) was used to perform the experiment. The protein-chromatin immuno-complex was washed 4 times to remove non-specific binding. Enrichment of promoter DNA was measured using the % input method by qRT-PCR analysis (Yamaguchi et al., 2014). Amplification of *ACTIN2* promoter sequence served as negative control. Primers for the ChIP-qPCR assays are in Table S2. The experiments were repeated for three biological repeats with similar results.

Small RNA extraction and gel blot analysis

Small RNAs were extracted as described (Qi et al., 2006). 3 g ground leaf powder was mix up with 8 mL Trizol (Takara, Cat#9108) and 3 mL chloroform. Then the supernatant was separated and collected by centrifugation followed by isopropanol precipitation. The RNAs in sediment were rinsed by 75% ethanol and dissolved in DEPC H_2O. To remove the mRNA, 30% PEG8000 and 5 M NaCl were used to deposit the mRNA, retaining the small RNAs in supernatant. Finally, these small RNAs were collected by ethanol precipitation. Gel blot analysis of sRNAs was performed as described (Qi et al., 2005). Briefly, 15 μg sRNA samples were separated by 15% denaturing gel electrophoresis and transferred onto Hybond-N^+ membranes (Amersham). DdH_2O was purified by Milli Q direct water purification system (Merck Millipore). Membranes were UV cross-linked and hybridized to ^{32}P-end-labeled oligonucleotide probes. The sequences of the probes are listed in Table S2. For detection of GFP/CLCuMuV/PPV derived siRNA, DNA fragments

were amplified by PCR with respective primers and labeled with BcaBest labelling kit (Takara, Cat#6046). For detection of CMV derived siRNA, oligo nucleotide probes are listed in Table S2. Experiments were repeated at least three times.

Protoplast transient expression assay

For transient transcriptional activity assay, the coding sequence of *CAMTA3* was cloned into pGreenII 62-SK vector under the control of the CaMV 35S promoter by ligation-independent cloning assay to generate effector construct. The upstream 2000-bp promoter sequences of *RDR6* and *BN2* were PCR-amplified by M5 Magic High-Fidelity DNA Polymerase (Mei5Bio, Cat#MF740) from genomic DNA and cloned into pGreenII 0800-*LUC* vector by ligation-independent cloning assay to generate the $RDR6_{Pro}$-*LUC* and $BN2_{Pro}$-*LUC* reporter construct. The "CGAT" mutant promoter sequences of *RDR6* and *BN2* were PCR-amplified from genomic DNA and cloned into pGreenII 0800-LUC vector to generate the $RDR6M_{Pro}$-*LUC* and $BN2M_{Pro}$-*LUC* reporter constructs. The Fast Mutagenesis Kit (ZOMANBIO, Cat#ZC401) was used to construct mutants. The pGreenII 62-SK vector and pGreenII 0800-LUC vector were described as (Hellens et al., 2005). All primers used for constructing these constructs are in Table S2. Protoplasts preparation and subsequent transfection were performed as described (Yan et al., 2018; Yoo et al., 2007). Firefly luciferase (LUC) and renillia luciferase (REN) activities were measured using the Dual-Luciferase Reporter Assay System (Promega, Cat#E1910) with a 96-well luminescence spectrometer (PerkinElmer EnVision). Relative LUC activity was calculated by normalizing against the REN activity. For all assays, 10 μg of reporter plasmid and effectors were used. All the experiments were repeated more than 3 biological times to calculate the Mean ± s.d. of relative ratio of LUC/REN.

In vitro enzymatic assay for BN2

To demonstrate miRNA-degrading activity of BN2, we expressed and purified glutathione S-transferase (GST)-tagged versions of BN2 (GST-BN2) and its mutant (GST-BN2M) with Ala-substitutions at Glu-143 and Asp-144 in the putative nuclease motif. The recombinant proteins were tested for nuclease activity *in vitro* using miRNA, ssDNA and RNA substrates. sRNA oligonucleotides corresponding to miR159, miR162, miR167, miR168 and miR403 with a 2'-O-methyl group and a 5'end-label was incubated with GST, GST-BN2, or GST-BN2M. The single-stranded miRNAs used in the assays were synthesized by Tsingke Technology Company. Following phenol/chloroform extraction they were 5'-end labeled with γ-^{32}P-ATP using T4 polynucleotide kinase (PNK; NEB) and subjected to enzymatic assays. Exonuclease activity assays were performed as described (Ramachandran and Chen, 2008). Reactions were carried out in a 20 μL mixture containing ^{32}P-labeled RNA or DNA substrates, 50 mM Tris-HCl pH 8.0, 135 mM KCl, 2.5 mM $MgCl_2$, 2.5% glycerol, BSA (1 μg/μL), RNasin (40 units; Promega), and purified GST-BN2, GST-BN2M protein or GST alone at 37°C for 1 hour. The amount of GST and GST-BN2M used in the reaction was 160 ng and 60 ng respectively. The amount of GST-BN2 was 20 ng (lanes 4 and B1), 40 ng (lanes 5 and B2) and 60 ng (lanes 6 and B3). Reactions were stopped by the addition of 20 μL loading dye as described (Qi et al., 2005). After denaturation at 95°C for 5 min, samples were resolved on denaturing polyacrylamide gels. For miRNAs gel blot analysis of Figures 3D and 3G, the reactions were analyzed on 15% denaturing polyacrylamide gels. For pre-miR168, the predicted pre-miR168 sequence from sRNAanno (http://plantsrna.org/) was PCR amplified with the forward primer encompassing a T7 promoter sequence. Following *in vitro* transcription by T7 RNA polymerase (Promega, Cat#P1300), the RNA was gel-purified, de-phosphorylated with alkaline phosphatase (CIP; NEB), and 5'-end labeled with T4 PNK prior to the enzymatic assay. For *ACTIN* mRNA, fragment of *ACTIN* cDNA was amplified by PCR with the forward primer encompassing a T7 promoter sequence and transcribed *in vitro*. The RNA was extracted with phenol/chloroform and precipitated. The RNA was de-phosphorylated using alkaline phosphatase (CIP; NEB), and 5'-end labeled with γ–^{32}P-ATP by T4 PNK prior to the enzymatic assays. For RNA gel blot analysis of Figure 3F, the reactions were analyzed on an 8% denaturing polyacrylamide gel. The single-strand DNA was synthesized by RUIBIO Technology Company with 3'-end labeled with biotin. DNA samples were separated on 1% agarose gel by electrophoresis and transferred onto Immobilon-NY$^+$ Charged Nylon (Merck Millipore) by downward alkaline gel blotting for 10 h. Hybridization and DNA membrane detection were performed by Chemiluminescent Hybridization and Detection Kit (Pierce, Cat#17097). Experiments were repeated at least three times.

QUANTIFICATION AND STATISTICAL ANALYSIS

Statistical significance of relative LUC/REN ratio, quantitative real-time PCR analysis were examined by Student's t-test (*$P<0.05$; **$P<0.01$). All of the statistical details of experiments can be found in the figure legends. All values for quantitative analysis was presented with means ± s.d. The number (n) of biological replicates was at least three. For quantification analysis, the intensities of bands were quantified with ImageJ.

ScienceDirect

Cell Host & Microbe

Volume 29, Issue 9, 8 September 2021, Pages 1393-1406.e7

Article

A calmodulin-binding transcription factor links calcium signaling to antiviral RNAi defense in plants

Yunjing Wang [1 2 9], Qian Gong [1 2 9], Yuyao Wu [1 2], Fan Huang [1 2], Asigul Ismayil [1 2], Danfeng Zhang [1 2], Huangai Li [1 2], Hanqing Gu [1 2], Márta Ludman [3], Károly Fátyol [3], Yijun Qi [1 2], Keiko Yoshioka [4], Linda Hanley-Bowdoin [5], Yiguo Hong [6 7 8], Yule Liu [1 2 10]

Show more

Outline | Share Cite

https://doi.org/10.1016/j.chom.2021.07.003

Get rights and content

Under an Elsevier user license

Open archive

Referred to by

Live imaging and quantitation of insect feeding-induced Ca^{2+} signal using *GCaMP3*-based system in *Nicotiana benthamiana*
STAR Protocols, Volume 3, Issue 1, 18 March 2022, Pages 101040
Yunjing Wang, Qian Gong, Fan Huang, Linfang He, Yule Liu
View PDF

Ca^{2+} kickstarts antiviral RNAi
Cell Host & Microbe, Volume 29, Issue 9, 8 September 2021, Pages 1339-1341
April DeMell, Savithramma P. Dinesh-Kumar
View PDF

Highlights

- Plants recognize wounding-triggered Ca^{2+} flux to prime antiviral RNAi defense
- CAMTA3 activates *RDR6*/*BN2* expression to enhance antiviral RNAi
- BN2 upregulates *AGO1/2* and *DCL1* RNA levels by degrading miRNAs
- Geminivirus proteins disrupt CaM-CAMTA3 interaction to suppress antiviral RNAi

Summary

RNA interference (RNAi) is an across-kingdom gene regulatory and defense mechanism. However, little is known about how organisms sense initial cues to mobilize RNAi. Here, we show that wounding to Nicotiana benthamiana cells during virus intrusion activates RNAi-related gene expression through calcium signaling. A rapid wound-induced elevation in calcium fluxes triggers calmodulin-dependent activation of calmodulin-binding transcription activator-3 (CAMTA3), which activates *RNA-dependent RNA polymerase-6* and *Bifunctional nuclease-2* (*BN2*) transcription. BN2 stabilizes mRNAs encoding key components of RNAi machinery, notably *AGONAUTE1/2* and *DICER-LIKE1*, by degrading their cognate microRNAs. Consequently, multiple RNAi genes are primed for combating virus invasion. *Calmodulin*-, *CAMTA3*-, or *BN2*-knockdown/knockout plants show increased susceptibility to geminivirus, cucumovirus, and potyvirus. Notably, Geminivirus V2 protein can disrupt the calmodulin-CAMTA3 interaction to counteract RNAi defense. These findings link Ca^{2+} signaling to RNAi and reveal versatility of host antiviral defense and viral counter-defense.

Graphical abstract